UNIVERSITY OF CALIFORNIA,
IRVINE

The Protective Role of Mitochondrial Akt1 Against the Development of Diabetic Cardiomyopathy

DISSERTATION

submitted in partial satisfaction of the requirements
for the degree of

DOCTOR OF PHILOSOPHY

in Biomedical Sciences

by

Albert Ta

Dissertation Committee:
Professor Ping H. Wang, Chair
Associate Professor Francesco Tombola
Professor Kenneth Baldwin
Associate Professor Qin Yang
Associate Professor Mei Kong

2021

DEDICATION

To Mom and Dad

TABLE OF CONTENTS

LIST OF FIGURES

ACKNOWLEDGMENTS

I would like to firstly thank my thesis advisor, Dr. Ping Wang. The completion of my degree was made possible by the mentorship, support, and countless opportunities he provided. I would also like to thank the other members of the Wang lab: Dr. Yumay Chen, Dr. Hank Chen, and Dr. Hugo Lin for the training and help that they have given me over the years.

I could not have completed my Ph.D. without the love and support of my friends. Thank you to Anastasia Ionkina, Gabriela Balderrama-Gutierrez, Cindy Shuai, Stephanie Wu, Amanda McQuade, Srikiran Chandrasekaran, Peter Chongpinitchai, Steven Yen, and Richard Truong for their close support.

To my collaborators, I would like to express my gratitude. It was a pleasure working with and learning from each and every one of you. Thank you to Dr. Kenneth Roos, Dr. Maria Jordan, Dr. Marcus Seldin, Dr. Ying Yang, and Dr. Lingyi Tang.

Financial supports for this dissertation were provided by The National Institutes of Health R01HL096987, The California Institute of Regenerative Medicine, The Pacific Life Foundation, The Ko Family Foundation, The Musco Foundation, The Iacocca Foundation, The Chao Family Foundation, and The Fatima Foundation.

CURRICULUM VITAE

Albert Ta

2012 BS in Biochemistry and Molecular Biology, University of California, Davis

2015 MBS in Biomedical Sciences, The Commonwealth Medical College

2021 Ph.D. in Biomedical Sciences, University of California, Irvine

Field of Study

Mitochondria, Cellular Metabolism, Cell Signaling Transduction, and Diabetic Cardiomyopathy

Publications

Elucidation of WW domain ligand binding specificities in the Hippo pathway reveals STXBP4 as YAP inhibitor. Vargas RE, Duong VT, Han H, **Ta AP**, Chen Y, Zhao S, Yang B, Seo G, Chuc K, Oh S, El Ali A, Razorenova OV, Chen J, Luo R, Li X, Wang W. EMBO J. 2020 January.

Hybrid Two-Component Sensors for Identification of Bacterial Chemoreceptor Function. Luu RA, Schomer RA, Brunton CN, Truong R, **Ta AP**, Tan WA, Parales JV, Wang YJ, Huo YW, Liu SJ, Ditty JL, Stewart V, Parales RE. Appl Environ Microbiol. 2019 October.

Regulation of the Hippo Pathway by Phosphatidic Acid-Mediated Lipid-Protein Interaction. Han H, Qi R, Zhou JJ, **Ta AP**, Yang B, Nakaoka HJ, Seo G, Guan KL, Luo R, Wang W. Mol Cell. 2018 October.

Decreased incidence of diabetes in patients with gout using benzbromarone. Niu SW, Chang KT, **Ta A**, Chang YH, Kuo IC, Hung CC, Chiu YW, Hwang SJ, Lin SF, Lin HY.Rheumatology (Oxford). 2018 September.

Proteomic Analysis of the Human Tankyrase Protein Interaction Network Reveals Its Role in Pexophagy. Li X, Han H, Zhou MT, Yang B, **Ta AP**, Li N, Chen J, Wang W. Cell Rep. 2017 July.

Presentations

Albert Ta, Yu-Han Chen, Yumay Chen, Hyejin Lee, Hugo Y. Lin, Hsiao-Chen Lee, Ping H. Wang. Investigating the Protective Effects of Mitochondrial Akt1 Signaling against Diabetic Cardiomyopathy. UC Irvine School of Medicine Graduate Day. UCI. November 2017.

Albert Ta, Yu-Han Chen, Yumay Chen, Hsiaochen Lee, Hugo You-Hsien Lin And Ping H. Wang. Activation of Cardiac Mitochondrial Akt Signaling Improved Diabetic Cardiomyopathy and Induced Liver Metabolic Remodeling. American Diabetes Association 78th Scientific Sessions. June 2018.

Yu-Han Chen, Yumay Chen, **Albert Ta**, Hsiaochen Lee, Hugo You-Hsien Lin And Ping H. Wang. Remodeling of Myocardial Metabolism by Cardiac Mitochondrial Akt Signaling through Modulation of Pyruvate Dehydrogenase Complex. American Diabetes Association 78th Scientific Sessions. June 2018.

Yu-Han Chen, **Albert Ta**, Yumay Chen, Hsiaochen Lee, Hugo You-Hsien Lin And Ping H. Wang. Mitochondrial Akt in Myocardium Improved Heart Failure and Body Composition in A Mouse Model of Metabolic Syndrome with Reduced Insulin Secretion. American Diabetes Association 79th Scientific Sessions. June 2019.

Professional Organization Memberships

2017-Present: Member, Graduate Professional Success Biomed Program, UCI, CA.

ABSTRACT OF THE DISSERTATION

The Protective Role of Mitochondrial Akt1 Against the Development of Diabetic Cardiomyopathy

By

Albert Ta

Doctor of Philosophy in Biomedical Sciences

University of California, Irvine, 2021

Professor Ping H. Wang, Chair

Diabetic cardiomyopathy, the changes to myocardial structure and function directly attributed to diabetes, is increasing in prevalence, correlating with this rise of the diabetes and obesity epidemics. Despite this, the exact mechanisms are unclear and no specific treatments for diabetic cardiomyopathy (DCM) yet exists, thus the need for further research. Mitochondrial dysfunction is characteristic of DCM and we have demonstrated that impaired translocation of AKT1 to mitochondria due to insulin resistance in animal models of diet-induced diabetes, accompanied by changes of mitochondrial structure and function. Here we showed that maintaining mito-Akt1 signaling in the context of diet-induced diabetes protected against the development of DCM. I investigated the underlying mechanisms, using a novel cardiomyocyte-specific transgenic mice harboring an inducible mitochondria-targeting constitutively active AKT (CAMCAKT) with a Cre-lox strategy. Under a high fat, high fructose diet, diabetic CAMCAKT mice exhibited improved heart function, whereby ejection fraction was 17 % higher than in diabetic controls ($p < 0.05$) and fractional shortening was 22% greater ($p < 0.05$). Left ventricular hypertrophy and perivascular fibrosis was also significantly reduced ($p < 0.05$). Gene

expression analysis suggested that fatty acid. metabolism was upregulated by mito-Akt1 while simultaneously, extracellular flux assays measured improved respiratory efficiency coupled with increased myocardial ATP concentration ($p < 0.05$). Interestingly, improvements in heart function was associated with improvements in whole body metabolism, in vivo studies indicated increased energy expenditure ($p < 0.05$) and improved whole body leanness ($p < 0.05$). Liver steatosis was reduced ($p < 0.05$) in the CAMCAKT mice, furthermore, inter organ endocrine peptide analysis predicted remote modulation of liver metabolism by the heart. In summary, we showed a substantial role of cardiac mitochondrial AKT signaling during the development of DCM and demonstrated its metabolic and regulatory benefits in both the myocardium and also in whole body metabolism.

CHAPTER 1

Mitochondrial Akt1 in Diabetic Cardiomyopathy

I. Introduction

In recent decades, diabetes mellitus has become an epidemic and represents one of the most prevalent disorders in the developed world. Amongst diabetic patients, cardiovascular complications are the major cause of mortality and morbidity. It is now widely recognized that the risk for developing heart failure is significantly increased by diabetes. The changes in myocardial structure and performance directed attributed to diabetes, corrected for, or in the absence of other cardiac risk factors, such as coronary artery disease and hypertension, are defined as diabetic cardiomyopathy. Currently, no therapeutics exists to specifically treat diabetic cardiomyopathy, despite its increase in prevalence, thus, research into the mechanisms underlying the development of this disease is needed.

II. Background

Substantial evidence for diabetic cardiomyopathy as a clinical phenomenon was first published in a 1974 Framingham Heart Study which demonstrated that heart failure was five times more prevalent in diabetic women and more than two times more prevalent in diabetic men after normalizing for other risk factors such as age, coronary health, and blood pressure [1]. Recently, in 2013, the American Heart Association et al, defined diabetic cardiomyopathy as a clinical condition of ventricular dysfunction occurring in the absence of atherosclerosis and hypertension in patients with diabetes [2].

1. Epidemiology of Diabetes Related Heart Failure

The prevalence of diabetic cardiomyopathy continues to increase driven by the increase in the diabetes and obesity epidemics. In the United States, over 34 million individuals, or just over 10% of the population, has diabetes and an additional 25% of the population is considered to be prediabetic [3]. Clinical trials have shown that the prevalence of heart failure in diabetic patients ranges from 19-26% [4] [5] [6]. Studies have also found that in type 1 diabetes, every 1% increase in glycated hemoglobin A_{1C} is associated with a 30% increase in risk for heart failure, while in type 2 diabetes, it is an 8% increase in risk [7].

2. Clinical Features

Diabetic Cardiomyopathy is typically asymptomatic in its early stage of development, making diagnosis difficult. One of the first manifestations is left ventricle hypertrophy which may also be associated with decreased left ventricular compliance. Cardiomyocyte stiffness as well as myocardial fibrosis contribute to an enlarged ventricular septum and posterior myocardial wall thickness [8]. These structural changes result in impaired early diastolic filling, increase filling of the atrium, and prolonged isovolumetric relaxation [9]. Using, echocardiography and tissue Doppler imaging, these diastolic dysfunctions in are detected in 40-75% of diabetic patients [10] [11]. Late-stage diabetic cardiomyopathy is characterized by systolic dysfunction, leading to impaired blood ejection fraction and eventually, heart failure [12].

3. Biochemical Changes

Diabetes is characterized hyperglycemia resulting from defects in insulin secretion and or insulin action. As an insulin-sensitive organ, the heart is dependent on insulin signaling to maintain homeostasis and is both directly and indirectly impacted by altered insulin regulation and the associated hyperglycemic conditions. Several biochemical changes are proposed to contribute to the development of diabetic cardiomyopathy but there are numerous novel and emerging mechanisms.

Inflammation is a chronic condition of diabetes. Specifically, intramyocardial inflammation occurs in diabetic cardiomyopathy, triggered by high free fatty acid levels, impaired insulin signaling, and hyperglycemia, increases expression of vascular cell adhesion molecule 1 (VCAM-1), infiltration of leucocytes and macrophages, and expression of inflammatory cytokines (IL-1b, IL-6, IL-8, TNF-a, and TGF-b1) [13]. Pro-inflammatory signals contribute to cardiac oxidative stress, remodeling, fibrosis, and diastolic dysfunction [14]. Further studies are required to determine whether anti-inflammatory strategies will have clinical usefulness in humans.

Advanced Glycated End products are long-lived proteins that, due to exposure to sugar, becomes glycated, altering their structure and function [9]. Increased AGE formation due to hyperglycemia can cause crosslinks in collagen molecules, reinforcing the myocardial extracellular matrix stiffness, leading to decreased compliance. Cross-linked collagen also resists degradation by matrix metalloproteinases exacerbating myocardium wall stiffness [15]. Additionally, AGEs activate AGE receptors (RAGE) which upregulate the expression of NF-kB, contributing to a shift toward expression of b-myosin heavy chain, a marker of heart failure [16].

Fibrosis is a hallmark of diabetic cardiomyopathy observed both in humans and rodent models. Increased perivascular and intermyofibrillar fibrosis may be caused by a number of

mechanisms, including increased levels of AGEs previously mentioned [17]. Following injury to the myocardium, TGF-b levels are upregulated, stimulating the deposition of collagen by myofibroblasts in an attempt to repair the heart [18]. Simultaneously, matrix metalloproteinases, particularly, MMP-2, are inhibited, preventing the breakdown of collagen in the extracellular matrix, acceleration the development of fibrosis [19].

Altered Insulin Signaling profoundly alters cardiac function. Insulin binds to the insulin receptor on cardiomyocytes, activating insulin receptor substrate (IRS)-1/2 which in turns activates PI3K and, in turn, Akt. Akt stimulates glucose transporter GLUT4 translocation to the cell membrane, facilitating glucose uptake necessary to meet the high oxidative respiration demands of the myocardium [9]. Insulin signaling also promotes eNOS activation required for regulation of coronary microvascular flow [20]. Reduced PI3K and Akt signaling has been documented in diabetic patients and double IRS-1/2 models knockout rodent models which exhibited decrease cardiac uptake of glucose, decreased cardiomyocyte ATP content, and impaired cardiac metabolism [21] [22].

Mitochondrial dysfunction has been implicated in the pathogenesis of diabetes in virtually all insulin sensitive tissues and plays a critical role in the development of diabetic cardiomyopathy. Insulin signaling deficiency has been shown to impair mitochondrial respirative capacity, increase oxidative stress, and increase sensitivity to calcium handling [23].

Fatty acid uptake and oxidation is increased in animal models as well as in human cases of type 1 and 2 diabetes [24]. This is likely due to the elevated levels of serum fatty acid and triacylglycerol levels promoting lipid uptake into cardiomyocytes in conjunction with reduced glucose uptake due to impaired insulin stimulated GLUT4 glucose import [23, 25]. The altered metabolism in diabetic hearts results in decreased cardiac efficiency-an increase in myocardium

oxygen consumption, without an in equivalent increase in cardiac contractility [26]. Decreased cardiac efficiency suggests uncoupling of mitochondrial ATP synthesis from the depletion of the inner membrane proton gradient. A less well understood consequence of increased lipid uptake is lipotoxicity from the accumulation of lipid intermediates, such as ceramides, oxidized phospholipids, and diacylglycerol [27]. Paradoxically, attenuation of lipotoxicity has been demonstrated by increasing mitochondrial fatty acid oxidation [28]. Animal models in which triacylglycerol formation from fatty acid and fatty acid oxidation are upregulated have both been shown to attenuate lipid-induced cardiac dysfunction [29, 30].

Elevated oxidative stress caused by reactive oxygen species (ROS) has been demonstrated in the diabetic myocardium and is widely accepted as an important factor in the progression of cardiac damage. ROS can damage proteins, phospholipids, and DNA by oxidation [31]. In addition, elevated ROS also increases the formation of AGEs, PKC signaling, and inhibits the synthesis of eNOS and prostacyclin, all contributing to cardiomyopathy [27]. Mitochondrial ROS are a natural byproduct of oxygen metabolism in the complexes I and III of the mitochondrial electron transport chain [32]. Under hyperglycemic conditions, insulin resistance causes an increase in NADH and FAD flux to the mitochondrial respiratory chain, hyperpolarizing the inner membrane and consequently, inhibiting complexes I and III, resulting in excess ROS production [26].

Mitochondrial dysfunction as a critical mechanism of the development of diabetic cardiomyopathy will be explored in depth as the focus of this dissertation.

4. Diagnosis

Evaluating asymptomatic diabetic patients, in the absence of risk factors, continues to be a clinical challenge. Thus far, no serum biochemical profile for the development of diabetic cardiomyopathy has been established [33]. However, a selection of biomarkers has been proposed, including MMP-3, osteopontin, and BNP [34]. An emerging technology that may become a useful diagnostic tool is MRI in conjunction with labeled free radicals in order to track the source and product free radicals produced by the diabetic heart [34]. MRI with labeled fatty acid has also been shown to be useful in tracking cardiac uptake and accumulation of fatty acids, upregulated in diabetic conditions [35].

Currently, there exists no targeted treatment for diabetic cardiomyopathy. Glycemic control is the primary means of treatment for diabetes. However, despite the risk of heart failure increasing linearly with blood glucose levels, clinical studies have not yet concluded which, if any, method of glycemic control improves the outcome of heart failure [36]. Aside from diabetes prevention, further research is required to identify specific targets that maybe used to attenuate or prevent the development of diabetic cardiomyopathy

5. Mitochondrial Akt

Mitochondria are the most abundant organelles in cardiomyocytes due to their high cellular energy demands. Mitochondrial oxidative phosphorylation is responsible for meeting 95% of this energy demand. Diabetic cardiomyopathy has been observed in both Type 1 and 2 diabetic patients and both suffer from a reduced phosphocreatine/ATP ratio, indicating that a common perturbation maybe the cause of metabolic dysregulation in both diseases [37].

Insulin receptor signaling plays a key role in the regulation of myocardial oxidative phosphorylation. Insulin receptor KO mice have demonstrated decreased oxidative

phosphorylation and ventricular dysfunction. When activated by insulin, its receptor's substrate interacts with numerous signaling pathways, of which, the phosphatidylinositol-3-kinase/protein kinase B (PI3K/Akt) pathway is our group's focus. Akt is a serine/threonine kinase directly downstream of PI3K responsible for the majority of insulin's metabolic actions [37].

Our lab's prior research demonstrated that the reduction of the mitochondrial oxidative phosphorylation complex activities was responsible for the metabolic perturbations caused by diabetes. In a streptozotocin induced diabetic mouse model (STZ-DM), electron transport chain complexes I and III activity were moderately reduced while complex V activity was significantly reduced by 36%. In addition, the mitochondrial content in the diabetic myocardium was also found to be reduced. Taken together, the resultant complex V activity at the tissue level was 47% reduced compared to controls. Insulin administration was able to improve complex V activity in the STZ-DM mice while glucose control using Phlorizin, a renal tubule Na-glucose transporter inhibitor, was not. This is evidence that the reduction in oxidative phosphorylation caused by diabetes is mediated by impaired insulin deficiency and not by hyperglycemia [37].

We further investigated the mechanistic link between insulin deficiency and impaired mitochondrial oxidative phosphorylation, looking specifically at the mitochondrial signaling of protein kinase B (Akt). After administration of insulin into C57BL/6 mice, mitochondria were isolated from cardiac tissue and we found a significant increase in phosphorylated Akt. Residual cytosolic proteins were digested to prevent contamination and translocation of the insulin receptor as well as other downstream effectors, such as phospho-Erk were ruled out. To confirm that the effects of insulin signaling on mitochondrial oxidative phosphorylation were mediated by the PI3K-Akt pathway, mice were pretreated with LY294002, a PI3K inhibitor, and as expected, activation of Akt in mitochondria in response to insulin stimulation was blunted. We

concluded that insulin signaling induced acute translocation of phosphorylated Akt translocation into mitochondria in the myocardium [37].

Akt translocation to mitochondria is altered in the diabetic myocardium. Both STZ-DM model of type 1diabetes and a high fat, high fructose (HFF) model of diet induced type 2 diabetes were utilized. Insulin stimulation led to a significant increase in Akt translocation to mitochondria in STZ-DM mice while the increase in Akt translocation was not as dramatic in HFF mice. Thus, we demonstrated that insulin activated Akt phosphorylation in mitochondria paralleled insulin sensitivity [37].

Three isoforms of Akt are expressed in mammalian cells, two of which: Akt1 and Akt2 are predominantly expressed in the myocardium. We found that Akt1 was the only isoform to translocate to mitochondria upon insulin signaling. Upon entering the mitochondria, we found that phospho-Akt1 reached all mitochondrial compartments. 2 minutes after insulin stimulation, phospho-Akt1 reached the outer membrane and intermembrane space fractions of isolated mitochondria. Phospho-Akt1 was detected in inner membrane fractions of isolated mitochondria in samples collected 5-15 minutes after insulin stimulation. Thus, Akt1 stimulated translocation reaches the mitochondrial matrix [38].

Finally, we set to establish the causal link between mitochondrial Akt1 activation and complex V activity. We generated a constitutively active mitochondrial-targeting Akt1 expressing adenoviral vector which was used to transduce rat myocardia. The vector did not alter cytosolic Akt1 activity, but instead, localized to cardiac mitochondria. As a result of mitochondrial Akt1 signaling, complex V activity was increased by 24% while complex V abundance did not change [38].

Thus far, we have shown that insulin signaling promotes phospho-Akt1 translocation into the mitochondria, where it upregulates mitochondrial ATP output. Impairment in insulin signaling, both in vivo and in vitro blunts mitochondrial Akt1 translocation. To further investigate the effects and mechanisms of impaired mitochondrial signaling we generated an inducible bitransgenic mouse model capable of expressing a dominant negative mitochondrial Akt1.

III. Materials and Methods

1. Transgenic Mice

To achieve mitochondrial-targeting (mt-targeting), the sequence from human cytochrome c oxidase subunit 8A (NP_004065.1; MSVLTPLLLRGLTGSARRLPVPRAKIHSL) was added to the 5' end of the AKT1 cDNA. The mt-targeting sequence is removed during mitochondrial import. To generate a dominant-negative AKT1 (mdnAKT), K179 was mutated to methionine to abolish ATP binding. To mediate cre-conditional expression of mdnAKT in mice, each coding sequence was first cloned into pCALNL-dsRed; pCALNL-DsRed was a gift from Dr. Constance Cepko (Addgene plasmid # 13769) following removal of the Ds-Red coding sequence.

In pCALNL a CMV immediate early gene enhancer and chicken beta-actin gene promoter/intron and beta-globin polyA signal drives expression of a coding sequence following cre-mediated deletion of a floxed PGK-neo-polyA sequence between the promoter and the coding sequence. To mediate targeting to the ROSA26 (Gt(ROSA)26Sor) locus, mdnAKT was independently cloned into pROSA26-1, a gift from Dr. Philippe Soriano (Addgene plasmid # 21714) with the CAG promoter oriented opposed to the ROSA26 lnc RNA transcript.

JM8.N4 ES cells (derived from C57BL/6NTac mice) were electroporated with linearized targeting constructs and 32 G418-resistant clones for each construct were screened for

homologous recombination. Targeting efficiency was 50% for the mdnAKT construct. Correctly targeted ES cells were microinjected into C57BL/6J blastocysts and the resulting male chimeras were bred with C57BL/6 mice to establish the lines used in this study. Engineering of mES cells, genomic characterization, microinjection of blastocysts and production of founder transgenic mice were carried out at the UCI Transgenic Mouse Facility.

To mediate inducible overexpression of mdnAKT in cardiomyocytes, ROSA26-CAG-LNL-mdnAKT mice were crossed with a cardiomyocyte-specific, myosin heavy chain 6 driven-Cre transgenic mouse strain (Myh6/CreER^{T2}) to generate CAMDAKT mice. Mice were kept in a temperature-controlled environment, and fed ad libitum with laboratory chow (2020X, Envigo Teklad, UK). To induce AKT1 transgene expression, 8-week-old CAMDAKT heterozygous, and control mice were treated with a single injection of Tamoxifen (TAM), 50 mg/kg body weight. Expression of transgene was verified within 12 hours and thereafter. The experimental protocol was approved by the Institutional Animal Care and Use Committee at the University of California at Irvine (AUP-18-113) and the experiments were performed in accordance with federal and local guidelines.

2. Immunofluorescence

Paraffin-embedded kidney sections were deparaffinized with xylene and rehydrated with graded ethanol. For antigen retrieval, the slides were immersed in 0.1M Tris (pH 10) buffer and heated with a 1100 W GE microwave oven for three 3-min cycles at power levels of 5, 4 and 3. After cooling, the slides were rinsed with PBS. The tissue sections were circled with a liquid Blocker Super Pap Pen before incubating in anti-His-Tag antibody His-Tag (D3I1O)XP®

(diluted in 1XPBS, 4% BSA, 0.1% Triton X-100) and incubated overnight in a humified chamber at 4°C.

After extended washes with PBS, fluorescence-conjugated secondary antibodies were applied and placed in a humidified chamber, incubated in a GE microwave oven at power level 4 for 3 minutes, rinsed with PBS and stained with Mitotracker (10 nM) and DAPI (1 ug/ml) for 20 minutes at room temperature. After washing with PBS, the slides were mounted for analysis with Keyence BZ-X810 Inverted Microscope (Keyence, Osaka, Japan).

3. Western Blotting

The mitochondrial fractions were dissolved in 2% lauryl maltoside solution supplemented with 10% SigmaFAST^{TM} protease inhibitor (Sigma-Aldrich, S8820). Protein contents were determined with an Eppendorf BioPhotometer by Bradford assay. Equal amounts of proteins from each sample were resolved with 10% SDS-polyacrylamide gel and then transferred onto polyvinylidene difluoride membranes. The membranes were blocked with 5% fat-free milk or 5% BSA for one hour before incubation with primary antibodies overnight at 4^{o} C, washed three times with TBS-T (20mM Tris–HCl,pH7.5, 0.5 mM NaCl, and 0.1% Tween 20), incubated with anti-rabbit IgG, horseradish peroxidase -linked antibody (#7074) (1:2000 dilution in 5% fat-free milk or 5% BSA), washed three times with TBS-T (define what this is), and then incubated with West Pico Chemiluminescent Substrate to visualize the proteins (Thermo Scientific, Pittsburgh, PA). The images were acquired with a Syngene G:BOX and analyzed with ImageJ.

4. Masson's Trichrome Staining

Tissue samples were fixed overnight in 10% buffered formalin at 4°C, washed twice with phosphate-buffered saline (PBS), incubated in 65% and 70% ethanol, and progressively dehydrated with graded ethanol and Histoclear (National Diagnostics) with a Leica TP1020 tissue processor, and embedded in paraffin. 4 um paraffin sections were deparaffinized in xylene and rehydrated in graded ethanol. The sections were mordant in Bouin's solution (picric acid, formaldehyde, and acetic acid) overnight. After washing, they were stained with Weigert's Iron Hematoxyline Solution for 30 minutes, followed by Biebrich Scarlet-Acid Fucshin for 15 minutes, phosphomolybdic-phosphotungstic acid solution for 10 minutes, and then aniline blue for 20 minutes. After brief submersion in 0.5% acetic acid, the slides were dehydrated with 95% alcohol, 100% alcohol, and xylene. Images were captured with a Zeiss AxioPlan2 microscope and analyzed with AxioVision Rel 4.6 software or with a Keyence BZ-X810 Inverted Microscope (Keyence, Osaka, Japan) and analyzed with Keyence BZ-X800 Analyzer software.

IV. Results

1. Generating a Model of Cardiac Mitochondrial Targeting Dominant Negative Akt1

In order to further study the mechanisms of diabetic cardiomyopathy development, we set out to model the effects of impaired cardiac mitochondrial Akt1 signaling in an inducible animal model. To this end, we generated a mitochondria-targeting Dominant Negative Akt1 construct (mdn-Akt1) consisting of an Akt1 transcript with a K179 to M179 mutation. This point mutation prevents Akt1 kinase activity by inhibiting ATP binding. A 6X His tag sequence was inserted into the C terminus to allow for detection and pull down of the mutant Akt1 protein and a mitochondrial targeting sequence was added to the N terminus to ensure proper translocation.

Once in the mitochondria, the targeting sequence would be cleaved off endogenously (Figure 1.1).

The mdn-Akt1 construct was then cloned in frame, downstream of a floxed neomycin resistance sequence and CAG promoter and inserted into the Rosa26 locus of a C57BL/6 mouse. This transgenic mouse was then crossed with a transgenic mouse harboring Cre recombinase driven by a cardiomyocyte-specific myosin heavy chain 6 promoter (Myh6/CreER^{T2}). Cre recombinase is continually expressed in cardiomyocytes but only enters the nucleus to drive recombination upon the administration of tamoxifen. The result is a bi-transgenic model of heart-specific inducible, dominant negative mitochondria-targeting Akt1, referred to as CAMDAKT (Figure 1.2).

2. DNMKAKT Model Expression is Inducible and Heart Specific

Our bi-transgenic model is complex and as a result, careful steps were taken to validate our construct to ensure that expression is only induced upon tamoxifen administration (TAM) and is limited to cardiomyocytes. Immunofluorescence images were taken of paraffinized heart sections from CAMDAKT mice injected with either tamoxifen or corn oil, as a vehicle control. The sections were stained with MitoTracker, for the identification of mitochondria and 6X His-tag antibody for detection of the mdn-Akt1 protein (Figure 1.3A). No expression of His-tag was detected in samples from corn oil injected CAMDAKT mice. Samples from TAM CAMDAKT mice showed expression of His-tag, colocalizing with mitochondria, indicating proper expression and targeting of the dominant negative Akt1. Western blotting detection of 6X His-tag confirmed that dominant negative Akt1 expression occurs only when CAMDAKT are injected with tamoxifen and not expressed in wild type or Myh6/CreER^{T2} mice (Figure 1.3B). Furthermore,

expression of dominant negative Akt1 only occurs in the heart. These results confirmed that our model of cardiac-specific mitochondria-targeting dominant negative Akt1 is expressed as intended.

3. Dominant Negative mito-Akt1 caused Severe Fibrosis in CAMDAKT Mice

Masson's Trichome staining of heart sections show severe fibrosis occurring in TAM CAMDAKT mice only five days after induction of dominant negative Akt1 (Figure 1.4). This demonstrated that our model displays the expected phenotype of cardiomyopathy resulting from impaired Akt1 signaling.

4. Impaired Cardiac Mitochondrial Akt1 Signaling Severely Disrupted ATP Synthase and Mitochondrial Structure

Mitochondrial protein was isolated and centrifuged down a sucrose gradient column to separate proteins by mass. In total, 24 fractions were collected and blotted for the individual subunits of the ATP Synthase complex. Lower number fractions represented larger protein and protein complexes. In control mice, insulin injection increased the abundance of subunits: alpha, beta, gamma, delta, C and B1, in the lower number fractions, indicating their presence as part of a larger complex. In TAM CAMDAKT mice, insulin administration had no effect on the abundance of ATP Synthase subunits in higher protein size fractions (Figure 1.5A). These findings suggest that inhibition of mitochondrial Akt1disrupts insulin induced ATP Synthase complex composition.

Cryo-EM images of CAMDAKT are shown (Figure 1.5B). Corn oil injected CAMDAKT exhibited normal mitochondrial matrix structure wherein the folds are prominent and organized.

In TAM CAMDAKT mice, the cristae were disrupted, and organized folds were no longer visible. A schematic shows ATP Synthase's position, embedded in the inner mitochondrial membrane (Figure 1.5C). Impaired Atk1 compromised the integrity of the ATP Synthase complex and led to the unfolding of the cristae.

V. Discussion

Diabetic cardiomyopathy has only recently been established as a distinct clinical entity but has received more attention in recent years due to the rise in diabetes prevalence. The exact mechanisms are not known and there are current no drugs to specifically treat diabetic cardiomyopathy. Currently, traditional interventions for diabetes are used with limited effectiveness but further research is needed to develop more precise treatments.

Development of diabetic cardiomyopathy is linked to several factors stemming from insulin insensitivity and the hyperglycemic conditions characteristic of diabetes. The diabetic myocardium is in a chronic state of energy deficiency and mitochondrial dysfunction is a known to play a critical role on the pathogenesis of the disease. We have previously identified impaired Akt1 signaling to the mitochondria in the myocardium as a perturbation of normal cellular regulation, caused by insulin insensitivity. To investigate this link between diabetes and cardiomyopathy, we generated a novel transgenic mouse model expressing cardiac-specific dominant negative mitochondria-targeting Atk1 to specifically manipulate this mechanism of diabetic cardiomyopathy development. Our model was able to quickly induce a severe phenotype of cardiomyopathy by inhibiting mitochondrial Akt1 signaling, a process that normally would occur gradually over time as a result of chronic diabetes. In doing do, we were able to

demonstrate the substantial contribution mito-Akt1 signaling impairment plays in diabetic cardiomyopathy.

Our CAMDAKT model quickly developed myocardial fibrosis upon induction, a hallmark of late-stage diabetic cardiomyopathy. At the molecular level, we found a novel regulatory function for mitochondria bound activated Akt1- the maintenance of ATP synthase complexes. Without endogenous Akt1 signaling, there was significant dissociation of ATP synthase complexes, and in turn, loss of mitochondrial cristae, which undoubtedly reduced ATP production. Energy starvation as a driver of heart failure is a commonly accepted pathology. Therapeutic measures to reduce energy consumption, such as vasodilators and beta blockers, have shown improved survival in heart failure Conversely, treatments that increase energy demand on the heart, such as inotropes, worsen clinical outcomes, but few strategies to increase cardiac ATP supply have been tested [39]. High rates of heart failure ultimately led to poor survival rates of TAM CAMDAKT mice.

Having established mitochondrial Akt1 as a link between insulin insensitivity and heart failure, we next questioned if we could protect the heart against cardiomyopathy, using this same pathway.

VI. Figures

Figure 1.1

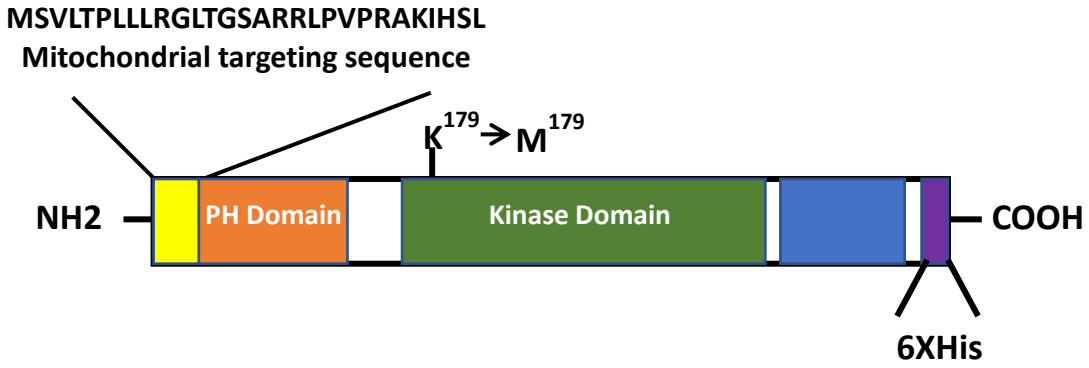

Figure 1.1 The Mitochondria-targeting Dominant Negative AKT1 Construct. Mitochondria targeting sequence was in frame fused to AKT1 cDNA at the N terminus. A 6X His was in-frame fused to the C terminus of AKT1 cDNA. To generate a dominant negative AKT1, the ATP binding site of AKT1, lysine 179 was mutated into methionine.

Figure 1.2

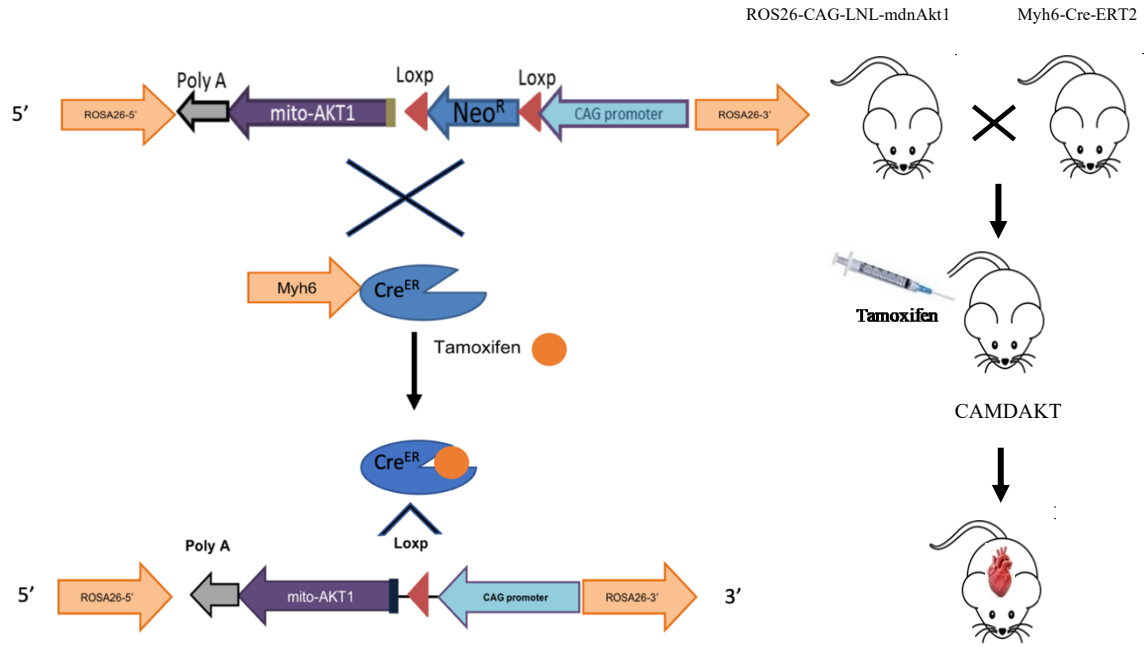

Figure 1.2 Design of Bi-transgenic Mice (CAMDAKT) for cardiac-specific Mitochondria-targeting Dominant Negative AKT1 (mdnAKT1) Expression. This is the scheme of the strategy to generate cardiomyocyte-specific overexpression of mitochondria-targeting dominant negative AKT1. A mitochondria-targeting sequence was inserted at the 5' end of the AKT1 cDNA with K179 mutated into Methionine. A mouse with Cre recombinase expressed cardiomyocyte-specific promoter myosin heavy chain 6 (Myh6/CreER^{T2}) was used to cross with mice harboring mdnAKT1 to generate bi-transgenic mice which mdnAKT1 expression can be induced by tamoxifen injection (CAMDAKT).

Figure 1.3

CAMDAKT

A.

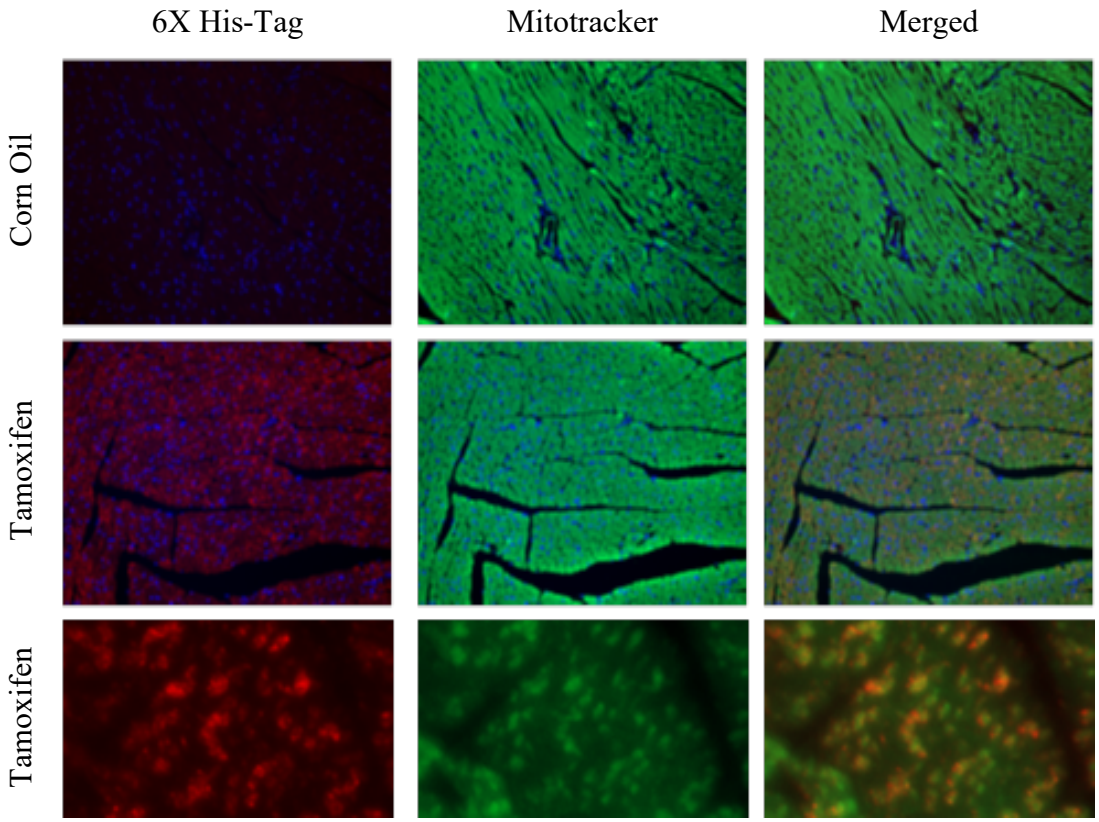

B.

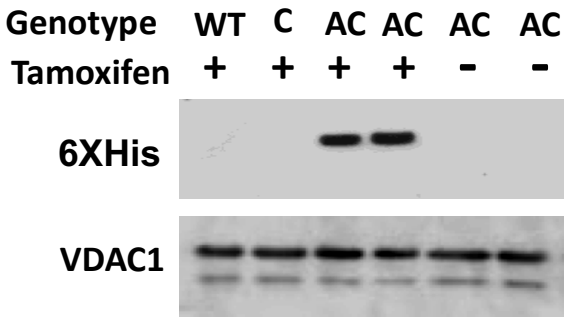

WT: Wild Type
A: mdnAkt
C: Cre

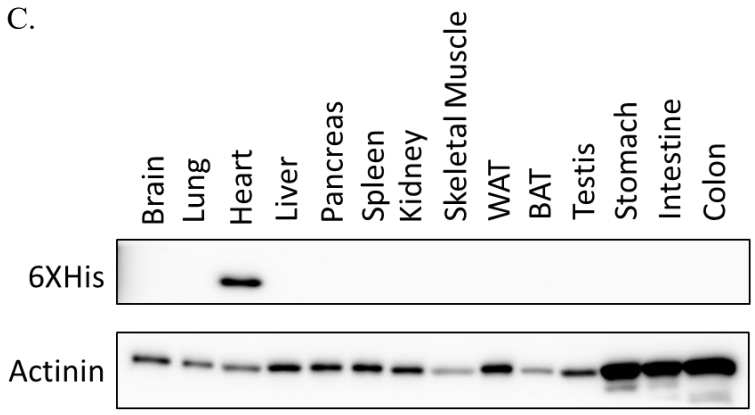

Figure 1.3 Inducible Mitochondria-targeting Dominant Negative AKT1 in Cardiomyocytes

Eight weeks old CAMDAKT mice were injected with tamoxifen (TAM) or corn oil. (A) Co-localization of mdnAKT and mitochondria in cardiomyocytes was demonstrated with IF staining with anti-His-Tag antibody (His-Tag (D3I1O)XP® and MitoTracker® Green FM (ThermoFisher Scientific) WT: wild type mice, CAMDAKT: bi-transgenic heart-specific mdnAKT mice. (B) Expression of the mdnAkt construct only occurs when CAMDAKT mice were injected with TAM and is not expressed in WT or Myh6/CreER^{T2} mice. (C) Expression of dominant negative Akt1 only occurs in the heart.

Figure 1.4

CAMDAKT

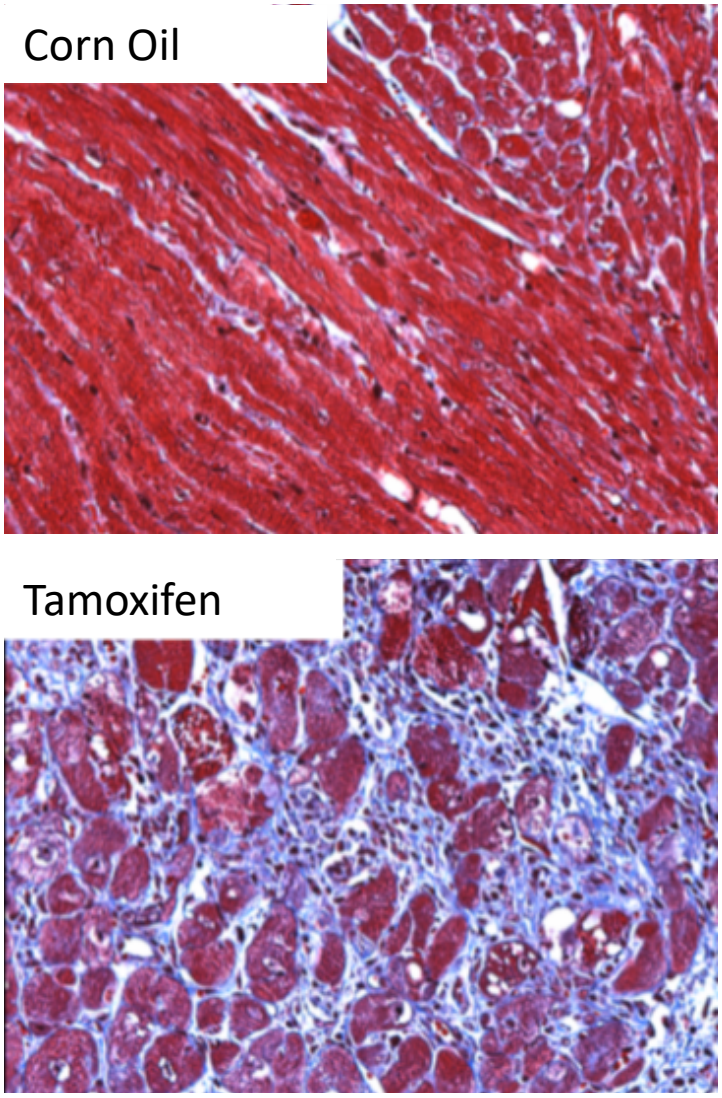

Figure 1.4 Impaired Cardiac Mitochondrial Akt1 Signaling Caused Severe Fibrosis

Representative images shown of cardiac sections of CAMDAKT mice stained with Masson's trichrome. Severe fibrosis resulted in CAMDAKT mice injected with TAM.

Figure 1.5

CAMDAKT

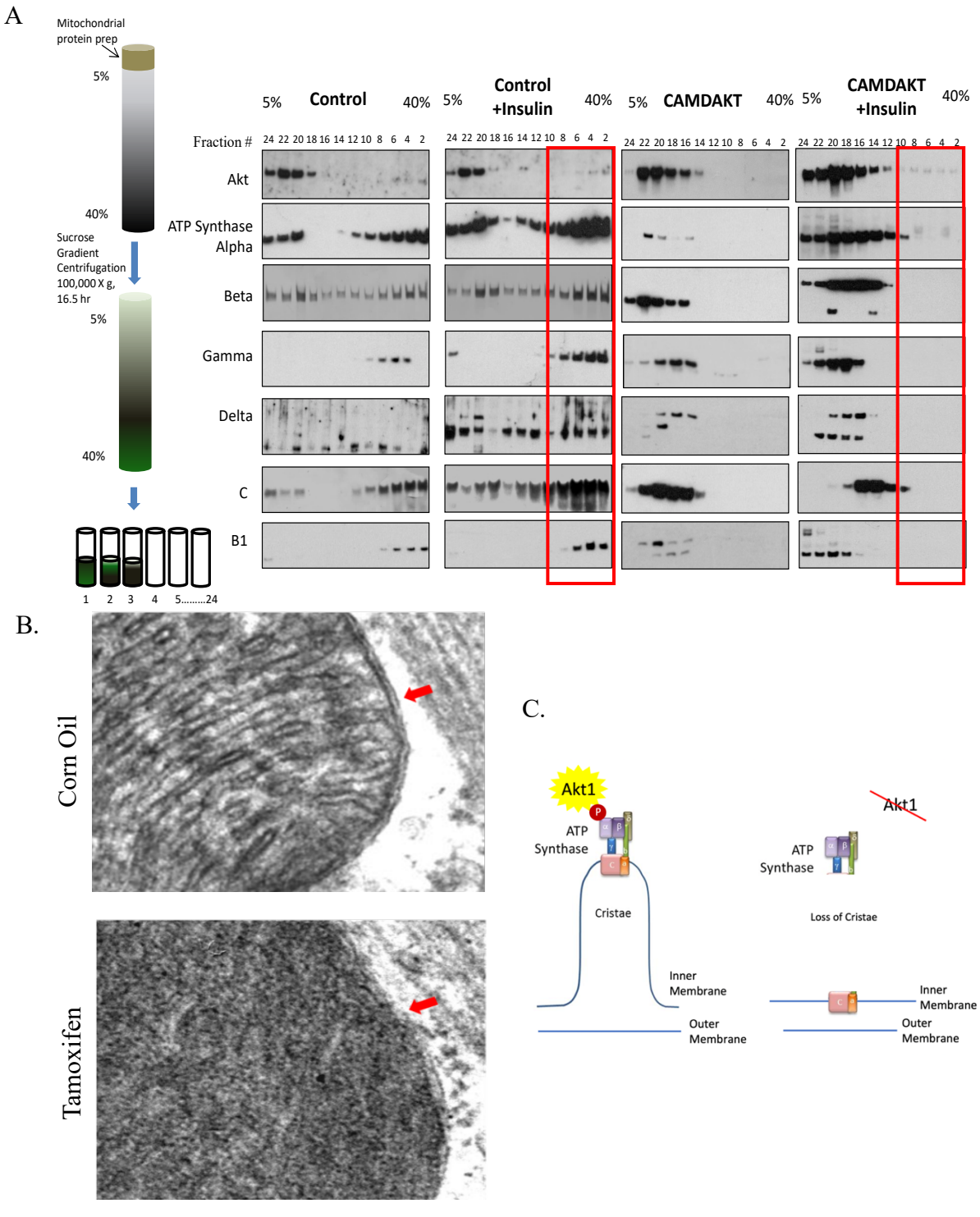

Figure 1.5 Impaired Cardiac Mitochondrial Akt1 Signaling Severely Disrupted ATP Synthase and Mitochondrial Structure. (A) Blot of ATP Synthase subunits separated by sucrose gradient are shown. Dominant negative mito-Akt1 signaling induced by TAM injection of CAMDAKT mice caused dissociation of ATP Synthase complexes. (B) Cryo-EM image showing loss of cristae in TAM injected CAMDAKT mice. (C) Schematic of ATP Synthase structure within inner mitochondrial membrane. Dissociation of the complex causes loss of mitochondrial matrix fold integrity.

CHAPTER 2

Activated Mitochondrial Akt1 Protected Against Diabetic Cardiomyopathy

I. Introduction

Building on our previous work in establishing impaired mitochondrial Akt1 signaling as a novel mechanism of development of diabetic cardiomyopathy, we asked if activated Akt1 could be protective against the disease. If mitochondrial Akt1 is a critical mechanism of this disease, we hypothesized that by maintaining its regulatory activity, in a diabetic condition, we could attenuate or even prevent the development of cardiomyopathy. To this end, we generated a bi-transgenic mouse model of constitutively active, cardiac-specific, mitochondria-targeting Akt1. This model allowed us to track the physiological effects of mitochondrial Atk1 on the development of diabetic cardiomyopathy as well as interrogate resulting the bioenergetic and molecular changes.

II. Materials and Methods

1. Transgenic Mice

To achieve mitochondrial-targeting (mt-targeting), the sequence from human cytochrome c oxidase subunit 8A (NP_004065.1; MSVLTPLLLRGLTGSARRLPVPRAKIHSL) was added to the 5' end of the AKT1 cDNA. To generate a constitutively active AKT (mcaAKT), threonine T308 and serine S473 were mutated to glutamic acid to mimic phosphorylation. To mediate cre-conditional expression of mcaAKT in mice, each coding sequence was first cloned into

pCALNL-dsRed; pCALNL-DsRed was a gift from Dr. Constance Cepko (Addgene plasmid # 13769) following removal of the Ds-Red coding sequence.

In pCALNL a CMV immediate early gene enhancer and chicken beta-actin gene promoter/intron and beta-globin polyA signal drives expression of a coding sequence following cre-mediated deletion of a floxed PGK-neo-polyA sequence between the promoter and the coding sequence. To mediate targeting to the ROSA26 (Gt(ROSA)26Sor) locus, mcaAKT was cloned into pROSA26-1, a gift from Dr. Philippe Soriano (Addgene plasmid # 21714) with the CAG promoter oriented opposed to the ROSA26 lnc RNA transcript.

JM8.N4 ES cells (derived from C57BL/6NTac mice) were electroporated with linearized targeting constructs and 32 G418-resistant clones for each construct were screened for homologous recombination. Targeting efficiency was 53% for the construct. Correctly targeted ES cells were microinjected into C57BL/6J blastocysts and the resulting male chimeras were bred with C57BL/6 mice to establish the lines used in this study. Engineering of mES cells, genomic characterization, microinjection of blastocysts and production of founder transgenic mice were carried out at the UCI Transgenic Mouse Facility.

To mediate inducible overexpression of mcaAKT in cardiomyocytes, ROSA26-CAG-LNL-mcaAKT mice were crossed with a cardiomyocyte-specific, myosin heavy chain 6 driven-Cre transgenic mouse strain (Myh6/CreER^{T2}) to generate CAMCAKT mice. Mice were kept in a temperature-controlled environment, and fed ad libitum with laboratory chow (2020X, Envigo Teklad, UK). To induce AKT1 transgene expression, 8-week-old CAMCAKT heterozygous, and control mice were treated with a single injection of Tamoxifen (TAM), 50 mg/kg body weight. Expression of transgene was verified within 12 hours and thereafter. CAMCAKT, control mice, and or wild type mice were placed on a high fat and high fructose diet (HFF) for a

period of two to five months. High fat chow was specified at 45% calorie from fat (TD.08811, Envigo Teklad Custom Diet, UK). Cage water was replaced with a 30% fructose solution (Sigma F0127-5KG). The length of HHF is specified per given experiment, chow and water were replaced at two week intervals. The experimental protocol was approved by the Institutional Animal Care and Use Committee at the University of California at Irvine (AUP-18-113) and the experiments were performed in accordance with federal and local guidelines.

2. Echocardiogram

Mice were screened by echocardiography at the Mouse Physiology Core Laboratory at the UCLA Department of Physiology. Cardiac function was evaluated by noninvasive ultrasound echocardiography under light isoflurane sedation (0.5–1.0%) to prevent movement and cardiodepression. Data were acquired using a two-dimensional-guided M-Mode and spectral Doppler imaging with a Siemens Acuson Sequoia Model C256 equipped with a 15L8 15-MHz probe (Siemens Medical Solutions, Malvern, CA). Mice were evaluated to obtain heart dimension and function measurements, including left ventricle (LV) chamber size, wall thickness, end-diastolic dimension, end-systolic dimension, LV fractional shortening, velocity of circumferential fiber shortening, and LV ejection fraction.

3. Perivascular Fibrosis Staining

Cardiac tissue sections were prepared and trichome stained as previously described. 10 images at 20x were captured by random sampling with a Zeiss AxioPlan2 microscope. Each image was then processed by ImageJ to determine the degree of fibrosis. Blue areas were quantified using the color threshold function in ImageJ. White pixels were counted by setting the

following threshold settings: Hue (135, 220), Saturation (0, 255) and Brightness (60, 210). Pixels under threshold were measured and considered total area of blue stained collagen. The area of collagen was then divided by total captured area giving a percentage of fibrosis by area.

4. RNA Isolation

30-50ug of tissue was used per sample for RNA isolation. Tissue sample was rinsed in PBS and homogenized in 700uL Trizol using a plastic microfuge tube pestle. Samples were incubated at room temperature for 5 minutes before adding 200uL chloroform and vortexed. After, samples were incubated for 3 minutes at room temperature before centrifugation at 12000g for 15 minutes at 4°C. The resultant top aqueous layer was transferred to a new tube and 500uL isopropanol added, mixed and incubated at room temperature for 10 minutes. After, samples were centrifuged at 12000g for 15 minutes at 4°C. The resulting pellet was washed with 500uL ice cold 80% ethanol and then centrifuged again at 10,000g for 10 minutes at 4°C. Supernatant was discarded, pellet was dried for 5 minutes and then resuspended in 20-50uL DEPC water.

5. Analysis of Mitochondrial O2 Respiration by Metabolic Flux Measurement

To measure mitochondrial function in cells, a Seahorse Bioscience XFe24 Extracellular Flux Analyzer (Seahorse Bioscience, North Billerica, MA) was utilized according to the manufacturer's protocol. Mitochondria were isolated from heart tissue as described previously. 10 ug of mitochondrial protein was plated onto each experimental well of a Seahorse XFe24 assay plate by centrifugation at 3000 rpm for 20 minutes. The wells were then filled to 500µL with 1X Mitochondrial Assay Solution (MAS) (The following solutions were used: 70 mM sucrose, 220 mM mannitol, 10 mM KH_2PO_4, 5 mM $MgCl_2$, 2 mM HEPES, 1.0 mM EGTA

and 0.2 % (w/v) fatty acid-free BSA, pH 7.2). Coupling assay metabolic substrate conditions were either 10mM Pyruvate/5 mM Malate or 25μM Palmitoyl Carnitine/1 mM Malate as per stated assay. After incubation at 37 °C for 8 minutes, the assay plate was loaded into the XFe24.

Two baseline measurements of oxygen consumption rate (OCR) were taken before sequential injection of following mitochondrial inhibitors and final concentration: ADP (40 mM), oligomycin (2.5 μg/ml), carbonilcyanide p-triflouromethoxyphenylhydrazone (FCCP) (4 μM) and rotenone (0.1 μM). Two measurements were taken after addition of each inhibitor. OCR values were automatically calculated and recorded by the Seahorse Wave Controller software. The basal respiration was calculated by averaging the two measurements of OCR before injection of inhibitors. The first measurement taken after injection of ADP was calculated as Stage 3 Respiration.

6. RNA Sequencing

RNA sequencing was performed by the UC Irvine Genomics High Throughput Facility. RNA was isolated from heart and liver tissue as previously described. Each sample submitted for sequencing was prepared by pooling equal RNA amounts from three mice of the same experimental conditions. RNA sequence was performed on an Illumina NovaSeq6000 on an S1 flow cell. 12 samples were run on each lane resulting in a read depth of more than 60 million. Reads were analyzed by CLC Genomics Workbench 20.0 (Qiagen).

III. Results

1. Generating a Model of Cardiac Mitochondrial Targeting Constitutively Active Akt1

To create a model of cardiac mitochondria-targeting constitutively active Akt1, we went back to our proven CAMDAKT model and made specific modifications. Based on the mdn-Akt1 construct, we instead mutated phosphorylation sites: threonine (T) 308 and serine (S) 473 to glutamic acid (E). This created a phosphomimetic mutant Akt1 which is functionally constitutively active: mca-Akt1 (Figure 2.1).

As before, the mca-Akt1 construct was cloned in frame, downstream of a floxed neomycin resistance sequence and CAG promoter and inserted into the Rosa26 locus of a C57BL/6 mouse. This transgenic mouse was then crossed with a transgenic mouse harboring Cre recombinase driven by a cardiomyocyte-specific myosin heavy chain 6 promoter (Myh6/CreER^{T2}). Cre recombinase is continually expressed in cardiomyocytes but only enters the nucleus to drive recombination upon the administration of tamoxifen. The result is a bi-transgenic model of heart-specific inducible, constitutively active mitochondria-targeting Akt1, referred to as CAMCAKT (Figure 2.2).

Expression of mutant Akt1 in CAMCAKT was verified using immunofluorescence imaging. Paraffinized heart sections from CAMCAKT mice injected with either tamoxifen or corn oil, as a vehicle control, are shown. The sections were stained with MitoTracker, for the identification of mitochondria and 6X His-tag antibody for detection of the mdn-Akt1 protein (Figure 2.3). No expression of His-tag was detected in samples from corn oil injected CAMCAKT mice. Samples from TAM injected CAMCAKT mice showed expression of His-tag, colocalizing with mitochondria, indicating proper expression and targeting of the constitutively active Akt1.

2. Modeling the Development of Diabetic Cardiomyopathy

In order to model the development of diabetic cardiomyopathy in CAMCAKT mice, we employed a method of diet-induced diabetes. At 8 weeks old, CAMCAKT mice are either induced with TAM injection to express constitutively active Akt1 or corn oil as a vehicle control. Henceforth, TAM injected CAMCAKT mice will be referred to as CA mice. The mice are then placed on a high fat and high fructose diet (HFF) as detailed above for lengths specified by each experiment. Corn oil injected CAMCAKT are placed on the same diet and serve as the controls for each respective experiment (Figure 2.4).

After 2 months on the HFF diet, all mice had significantly elevated resting glucose level of 200 mg/dl (Figure 3.3C). By the end of 5 months on the HFF diet, the average mouse weight was 55g. Diet induced diabetes and obesity mouse models have been well established and are utilized here to challenge our CAMCAKT mice.

3. Constitutively Active mito-Akt1 Protected Against Left Ventricular Hypertrophy

Heart dimensions were measured using echocardiography. Left ventricular hypertrophy is an early pathology of diabetic cardiomyopathy and was detectable over age matched, normal chow-fed mice. After 2 months on a HFF diet, CA mice hearts had a 10% lower posterior wall thickness ($p < 0.05$) (Figure 2.5A), and a 12% lower ventricle septum thickness ($p < 0.05$) (Figure 2.5B). Based on these measurements, left ventricle mass was calculated to be 0.25-fold lower in CA mice than controls ($p < 0.05$) (Figure 2.5C). Ventricular hypertrophy was reduced in CA hearts and not significantly different than age-matched control mice on a normal chow diet. Ejection fraction (Figure 2.4D) and fractional shortening (Figure 2.4E) were unchanged in CA mice and not significantly different than age-matched mice on a normal chow diet. Representative echocardiographic images are shown with measurements annotated (Figure 2.5F).

Constitutively Active mito-Akt1 protected against left ventricular hypertrophy in early cardiomyopathy development.

4. Mitochondrial Akt1 Promotes Cardiac Function

Echocardiogram was further used to measure live heart function to demonstrate the role of mitochondrial Akt1 on heart function. Ejection fraction, a measure of volumetric output from the left ventricle, and fractional shortening, a measure of the contractile capability of the left ventricle are here used as metrics for heart function. Higher values are indicative of a more optimally functioning heart.

CAMCAKT mice were placed on a HFF diet for 5 months before echocardiography measurements. The difference in heart function was significant; ejection fraction in CA mice was 17 % higher than in controls ($n = 6,8$, $p < 0.05$) (Figure 2.6A) while fractional shortening was 22% greater ($n= 6,8$, $p < 0.05$) (Figure 2.6B).

Meanwhile, CAMDAKT mice were kept on a normal chow diet and measured at 5 months of age. The difference in heart function was, again, significant. Ejection fraction in DN mice was 18 % lower than its respective age matched and normal chow controls ($n = 14,15$, $p < 0.01$) (Figure 2.6C) while fractional shortening was 23% lower than controls ($n = 14,15$, $p < 0.05$) (Figure 2.6D). Together these results clearly show that mitochondrial Akt1 signaling promotes heart function. Its protective role is clear in a diabetic setting and impairment of endogenous mitochondrial Atk1 signaling causes a dramatic reduction in heart function.

5. Constitutively Active mito-Akt1 Reduced Formation of Perivascular Fibrosis.

Perivascular fibrosis formation is characteristic of diabetic cardiomyopathy and is quantified here. Cardiac sections from CAMCAKT hearts were stained with Maison's Trichrome to colorize collagen fibers and images were captured by random sampling (Figure 2.7A). CA hearts had 50% less perivascular fibrosis compared to controls after 5 months on a HFF diet ($n = 12$, $p < 0.05$) (Figure 2.7B). Reduced fibrosis is an important phenotype demonstrating less severe cardiomyopathy as a result of mito-Akt1.

6. Constitutively Active mito-Akt1 Reduces Expression of Heart Failure Markers.

RNA expression of additional heart failure markers was quantified by qPCR (Figure 2.8) Collagen 1 ($p < 0.0001$) and Collagen 3 ($p < 0.001$) were significantly downregulated, recapitulating the previous histological findings of reduced fibrosis. Additional heart failure markers: ANF ($p < 0.05$), BNP ($p < 0.01$), and Myh7 ($p < 0.01$) were also found to be significantly lowered in CA mice compared to controls after 5 months on HFF diet. Taken together, these established markers clearly demonstrate the attenuation of cardiomyopathy resulting from cardiac mitochondrial Akt1 signaling.

7. Constitutively Active mito-Akt1 Improves Mitochondrial Respiration Efficiency.

Having established improvement in cardiomyopathy attributed to mito-Akt1 signaling, we sought to investigate the mechanisms by which Akt1 alters cardiac metabolism to yield improved function. After 2 months on HFF diet, mitochondria from CAMCAKT mice are isolated and bioenergetics were measured using an extracellular flux analyzer.

Two coupling assays were performed using either private/malate or palmitate/malate as an energy source. Under both energy substrates, mitochondria from CA mice exhibited lower

oxygen consumption rates for all induced mitochondrial states, compared to controls (Figure 2.8A, B). Non-mitochondrial oxygen consumption was identical for all samples, confirming equal protein loading amounts.

CA basal respiration was 25% lower than controls in the pyruvate/malate coupling assay and 15% lower in the palmitate/malate coupling assay ($n = 6$, $p < 0.05$) (Figure 2.8C). CA state 3 was 31% lower than controls in the pyruvate/malate coupling assay and 30% lower in the palmitate/malate coupling assay ($n = 6$, $p < 0.05$) (Figure 2.8D). Despite lowered oxygen consumption, ATP concentration in CA mitochondria were nearly 1-fold higher ($n = 6$, $p < 0.05$) (Figure 2.8E). Consistent with this finding, proton leak was found to be 22% lower in CA mitochondria on both pyruvate/malate and palmitate/malate substrates ($n = 6$, $p < 0.05$) (Figure 2.8F). These measurements together suggest that constitutively active mito-Akt1 has a profound impact on mitochondrial metabolism, promoting more efficient respiration.

8. Constitutively Active mito-Akt1 Promotes Fatty Acid Metabolism

RNA expression of several markers for fatty acid metabolism were upregulated in CA myocardium (Figure 2.10). Acaca, Acsm3, Scd catalyze synthesis of acyl-CoA. Adiponectin, a protein hormone, promotes fatty acid synthesis. Phospholipase A hydrolyzes phospholipids into fatty acids. UCP1 consumes energy for thermogenesis.

IV. Discussion

Our study design accurately modeled the development of diabetic cardiomyopathy. Under a high fat and high fructose diet, mice presented ventricular hypertrophy after 2 months, characteristic of early-stage cardiomyopathy. After 5 months, heart function was diminished, a

late-stage consequence of the disease. In both early and later time points, we confirmed that maintaining mitochondrial Akt1 signaling was able to reduce hypertrophy and improve cardiac function respectively. In fact, heart function in CA mice were comparable to similarly aged DN control mice which have been on a normal chow diet. Therefore, mito-Akt1 was able to effectively protect cardiac output from the detrimental effects of a chronic high calorie diet.

Changes to the myocardium were most dramatic after 5 months on the HFF diet, modeling late-stage cardiomyopathy. Perivascular fibrosis was significantly reduced at this time in CA mice and these results were recapitulated by reduced RNA expression of both collagen 1 and 3. Furthermore, expression of natriuretic peptides atrial natriuretic factor (ANF) and B-type natriuretic peptide (BNP) were significantly reduced. Natriuretic peptides ANF and BNP are produced by myocytes in the atria and ventricles, respectively, in response to myocardial strain due to increased pressure or an overload in output demand [40]. Natriuretic peptides function to promote natriuresis, diuresis, vasodilation to reduce blood volume and pressure to alleviate strain on the heart [41]. Elevated BNP is widely accepted as the gold standard biomarker for diagnosing heart failure [40]. Myosin heavy chain 7 (Myh7) is a newly characterized marker for heart failure and downregulated in CA mice. Myh7 is one of ten sarcomeric myosin motors and is only endogenously expressed during cardiac development. Animal studies in which Myh7 was overexpressed resulted in cardiac dilation, and cardiac failure [42]. Taken together, mito-Akt1 clearly mitigates heart failure.

Mitochondrial dysfunction is a major contributing factor to cardiomyopathy. Both human and animal studies have demonstrated that myocardial oxygen consumption and lowered cardiac efficiency in diabetic hearts [43]. Lowered efficiency is primarily due to mitochondrial uncoupling, or the loss of membrane potential, and in turn, oxygen consumption, that does not

contribute to oxidative phosphorylation of ATP [44]. A basal level of uncoupling is necessary for heat generation and regulatory functions, but uncoupling is significantly elevated in insulin deficient conditions [44]. In our model, mitochondria from CA mice had consumed significantly less oxygen in basal and stage 3 respiration. Simultaneously, ATP concentration was notably higher in CA mitochondria compared to controls while proton leak was reduced. This trend was true whether pyruvate or palmitate was given as a fuel source, suggesting that despite any diabetes-induced shifts in energy source –a dynamic combination of carbohydrates and fatty acids – that may occur, mitochondrial Akt1 signaling improves respiratory efficiency.

RNA expression of several metabolic and regulatory genes were upregulated in CA mice. The implications of their expression range from increasing metabolic activity to protective factors against cardiomyopathy.

While the heart is metabolically flexible, the primary fuel source remains to be fatty acid metabolism. The physiological balance of lipid uptake and oxidation prevents accumulation of excess lipids. Processes that affect cardiac function, including obesity, diabetes mellitus, ischemia, and most forms of heart failure led to altered fatty acid oxidation and often also to the accumulation of lipids. Failing hearts are associated with decreased oxidation and storage of long chain fatty acids, favoring the production of acyl-derived toxic intermediates [45]. Accumulation of certain lipid intermediates, such as ceramide and diacylglycerides (DAG) cause lipotoxicity and subsequent myocardial dysfunction. Ceramides inhibit insulin mediated activation of Akt by stimulating Protein Phosphatase 2A, an Akt inhibitor, while DAG blocks insulin signaling by deactivation of IRS-1[46]. Acyl CoA synthases catalyze the formation of acyl CoAs from fatty acids, activating them for oxidation in mitochondria. In both humans and animals, acyl CoA activity is reduced in the failing heart. In an Acyl coenzyme A synthetase-1 (ACSL1) knockout

mouse model, fatty oxidation was severely impaired and ventricular hypertrophy was induced along with upregulation of fetal genes [47]. Overexpression of ACSL1 in animal models reduced cardiac hypertrophy and yielded improved heart function [48]. In our model, several acyl CoA synthases are upregulated including Acetyl-CoA Carboxylase, Mitochondrial Acyl-CoA Synthetase, Stearoyl-CoA desaturase. These upregulated enzymes suggest a state of increased fatty acid flux in CA mice to fuel ATP synthesis and prevent mitochondrial lipotoxicity.

Further promoting fatty acid oxidation may have resulted from elevated adiponectin expression in CA mitochondria. Adiponectin is primarily expressed by adipocytes but its role in cardiomyocytes has more recently been studied. Adiponectin, a peptide hormone, improves both glucose metabolism and insulin resistance by activation of the adenosine monophosphate-activated kinase (AMPK) signaling pathway which, in turn, activates a number of metabolic proteins including acetyl coenzyme A carboxylase and GLUT4. Previous studies have found that adiponectin receptors are upregulated in STZ-induced diabetic mice, but adiponectin protein levels are unchanged [49]. Therefore, mitochondrial Akt1 may be a novel adiponectin modulator in a myocardium that is already primed for adiponectin signaling.

Unlike in the liver, the heart does not carry out de novo lipogenesis from glucose or amino acids. The fatty acid demands by the heart are met by uptake of fatty acids from circulation. Despite this, the heart still expresses fatty acid synthase (FAS), not for promoting energy storage, but instead, to synthesize regulatory phosphatidylcholine species [50]. In the myocardium, FAS inhibits calmodulin-dependent protein kinase II, an important regulator of cardiomyocyte L-type calcium channels FAS deficient mice exhibited hyperactivated L-type calcium channel leading to perturbed calcium homeostasis and cardiac arrythmia as well as development of fibrosis and

chronic inflammation [50]. FAS is upregulated in CA myocardium and may function to protect to myocardium.

Our study design successfully produced a phenotype of diabetic cardiomyopathy. By maintaining mitochondrial Akt1 signaling activity in our transgenic mouse model, we were able to attenuate development of cardiomyopathy in both early and late stages. We also demonstrated the energetic improvements supported by mito-Akt1. Thus, we have shown that mitochondrial Akt1 signaling is a critical mechanism in the pathogenesis of this disease. In addition to cardiomyopathy, diabetes causes metabolic dysfunction throughout the body. As a major metabolic organ, we questioned if, by optimizing heart function, metabolic improvements could emerge in other organ systems.

V. Figures

Figure 2.1

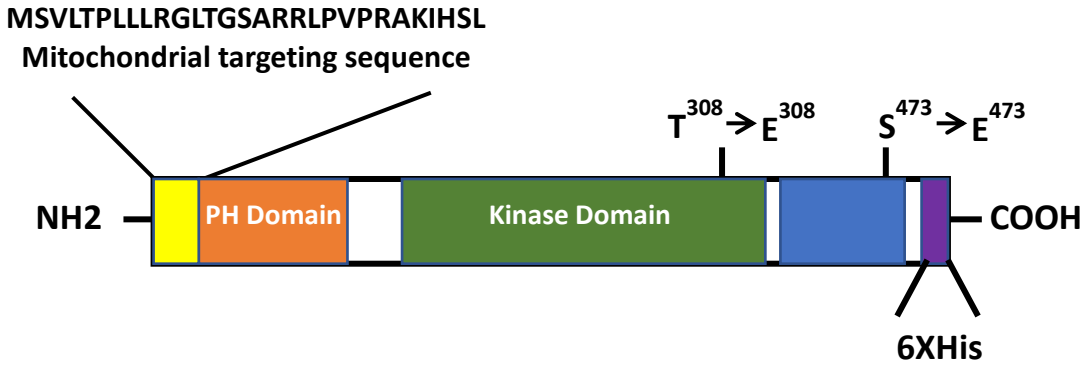

Figure 2.1 The Mitochondria-targeting Constitutive Active AKT1 Construct. Mitochondria targeting sequence was fused in frame to Akt1 cDNA at the N terminus. A 6X His was fused in frame to the C terminus of AktT1 cDNA. To generate the constitutive active Akt1, the Akt1 phosphorylation sites, threonine (T) 308 and serine (S) 473 were mutated to glutamic acid (E) to mimic phosphorylation.

Figure 2.2

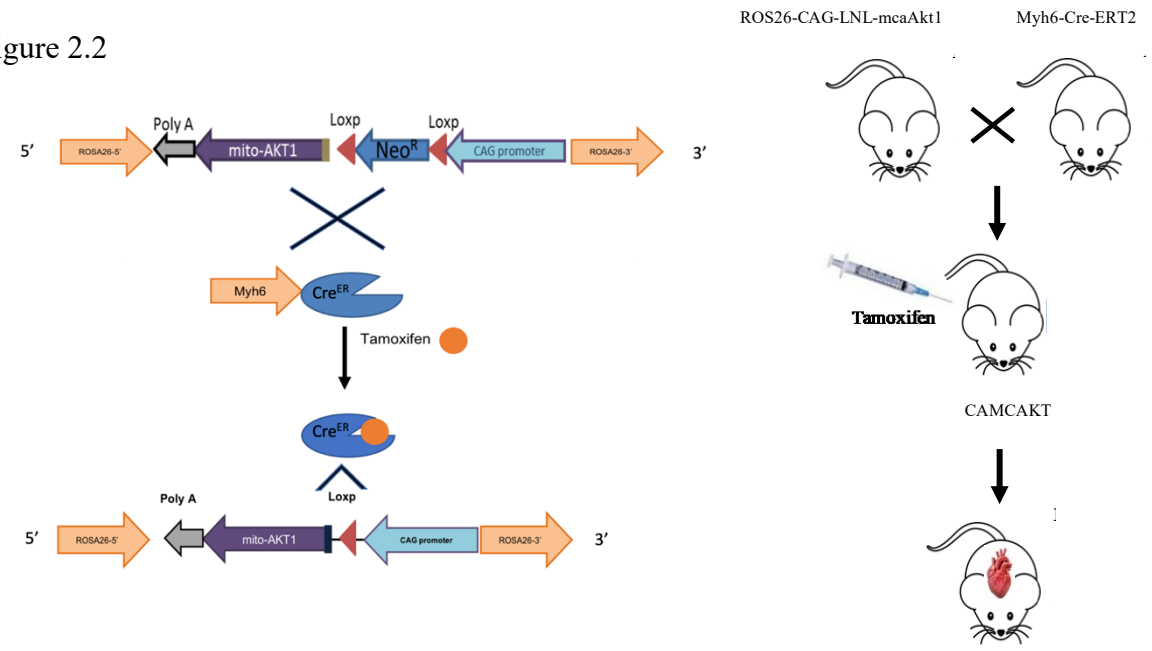

Figure 2.2 Design of Bi-transgenic Mice (CAMCAKT) for Cardiac Specific Mitochondria-targeting Constitutive Active AKT1 (mcaAKT1) Expression. This scheme outlines the strategy for cardiomyocyte-specific overexpression of mitochondria-targeting constitutive active AKT1. A mitochondria-targeting sequence was inserted at the 5' end of the AKT1 cDNA with T308 and S473 mutated into Glutamic acid. A mouse with Cre recombinase driven by cardiomyocyte-specific promoter myosin heavy chain 6 (Myh6/CreER^{T2}) was used to cross with mcaAKT1 mice, TAM injection induces mcaAKT1 in cardiomyocytes.

Figure 2.3

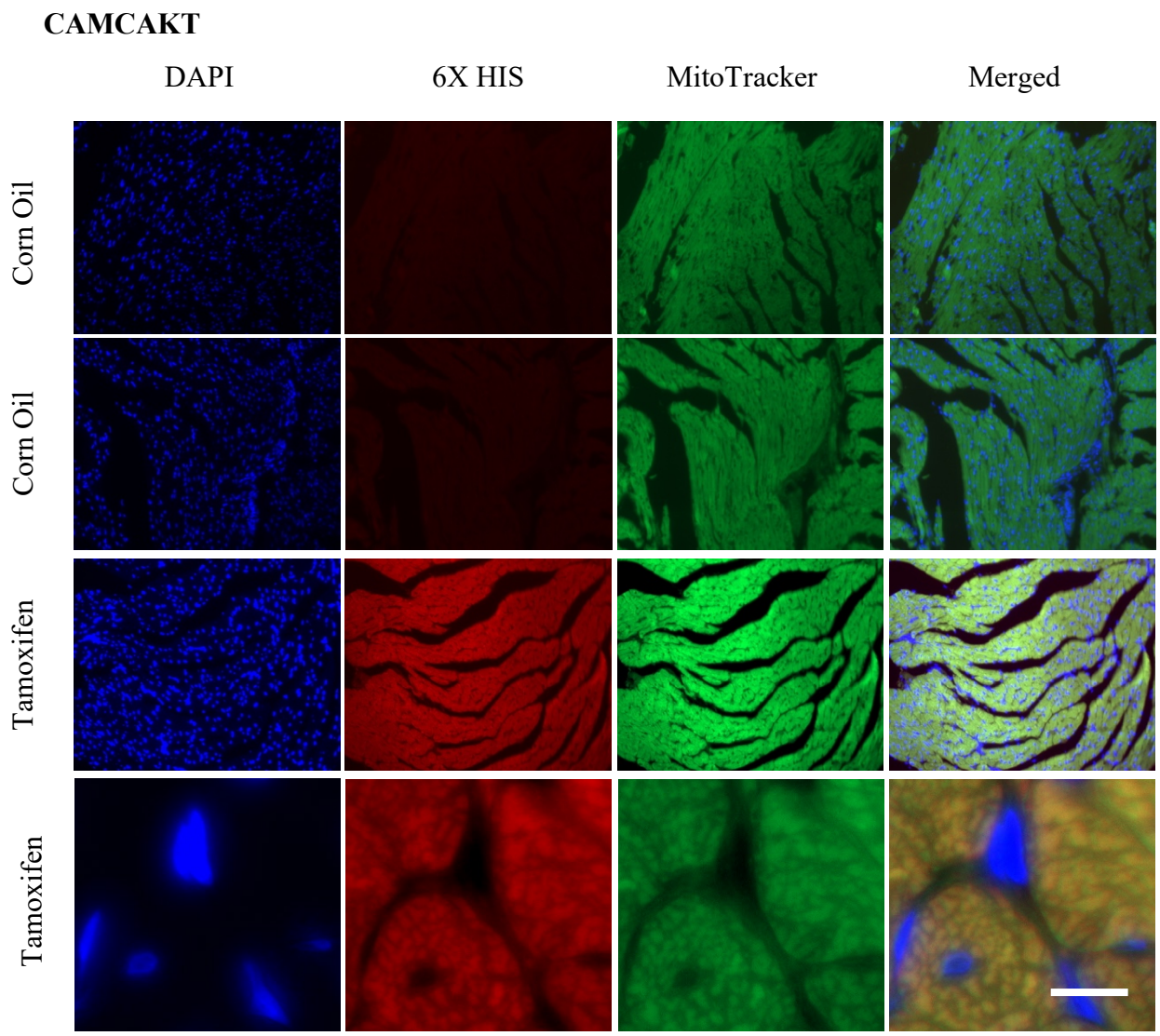
CAMCAKT
DAPI
6X HIS
MitoTracker
Merged
Corn Oil
Corn Oil
Tamoxifen
Tamoxifen
Bar: 50um

Figure 2.3 Cardiac-specific Expression of mcaAKT. CAMCAKT mice with inducible mitochondrial-targeting constitutive active AKT1 in cardiomyocytes were injected with tamoxifen (TAM) or corn oil at eight weeks old. Co-localization of mcaAKT and mitochondria in cardiomyocytes was studied by IF staining with anti-His-Tag antibody (His-Tag (D3I1O)XP® and MitoTracker® Green FM (ThermoFisher Scientific) WT: wild type mice, HCA: bi-transgenic heart-specific mcaAKT mice.

Figure 2.4

CAMCAKT

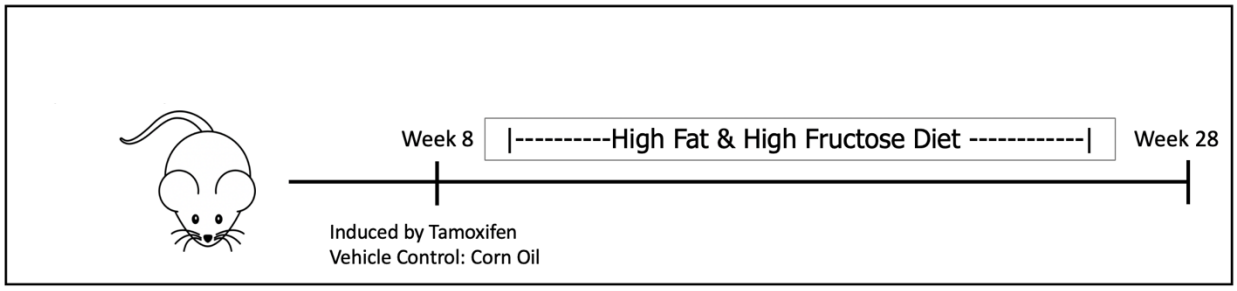

Figure 2.4 Study Design of Diabetic Cardiomyopathy Model To generate an animal model of diabetic cardiomyopathy, mice are placed on a high fat, high fructose diet at 8 weeks old. Expression of constitutively active mitochondrial-targeting Akt1 is induced in CAMCAKT mice by TAM injection (CA). Control mice are injected with corn oil (Control).

Figure 2.5

CAMCAKT

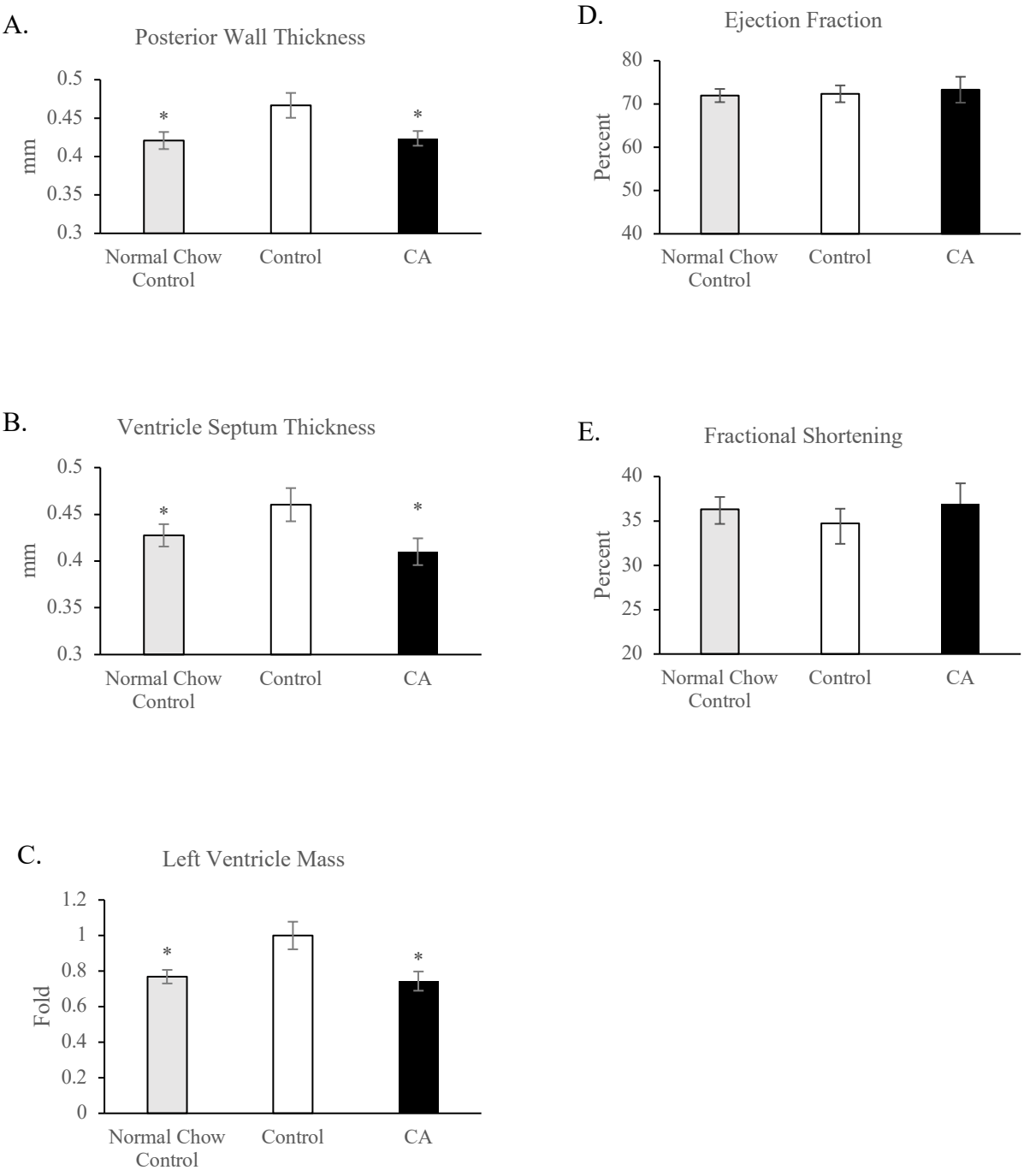

F.

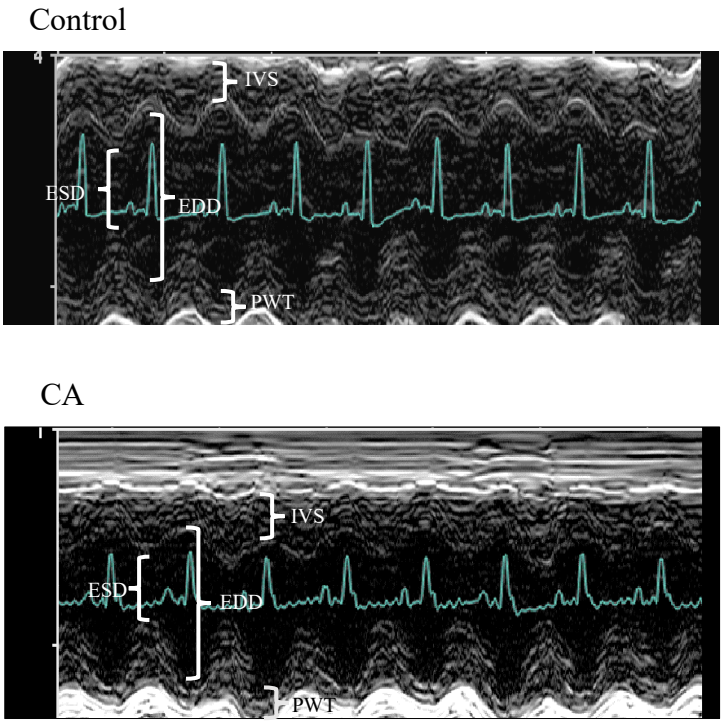

Figure 2.5 Constitutively Active mito-Akt1 Protected Against Left Ventricular Hypertrophy (A) Posterior Wall Thickness, (B) Ventricle Septum Thickness, and (C) Left Ventricle Mass were all lower in CA mice compared to controls after 2 months on HFF and equivalent to aged-matched mice on normal chow diet (n = 6, *p < 0.05). (D) (D) Ejection fraction and (E) fractional shortening were unchanged compared to controls on a HFF diet or normal chow. (F) Representative echocardiographic images shown with measurements of end diastolic diameter (EDD), end systolic diameter (ESD), interventricular septum (IVS), and posterior wall thickness (PWT).

Figure 2.6

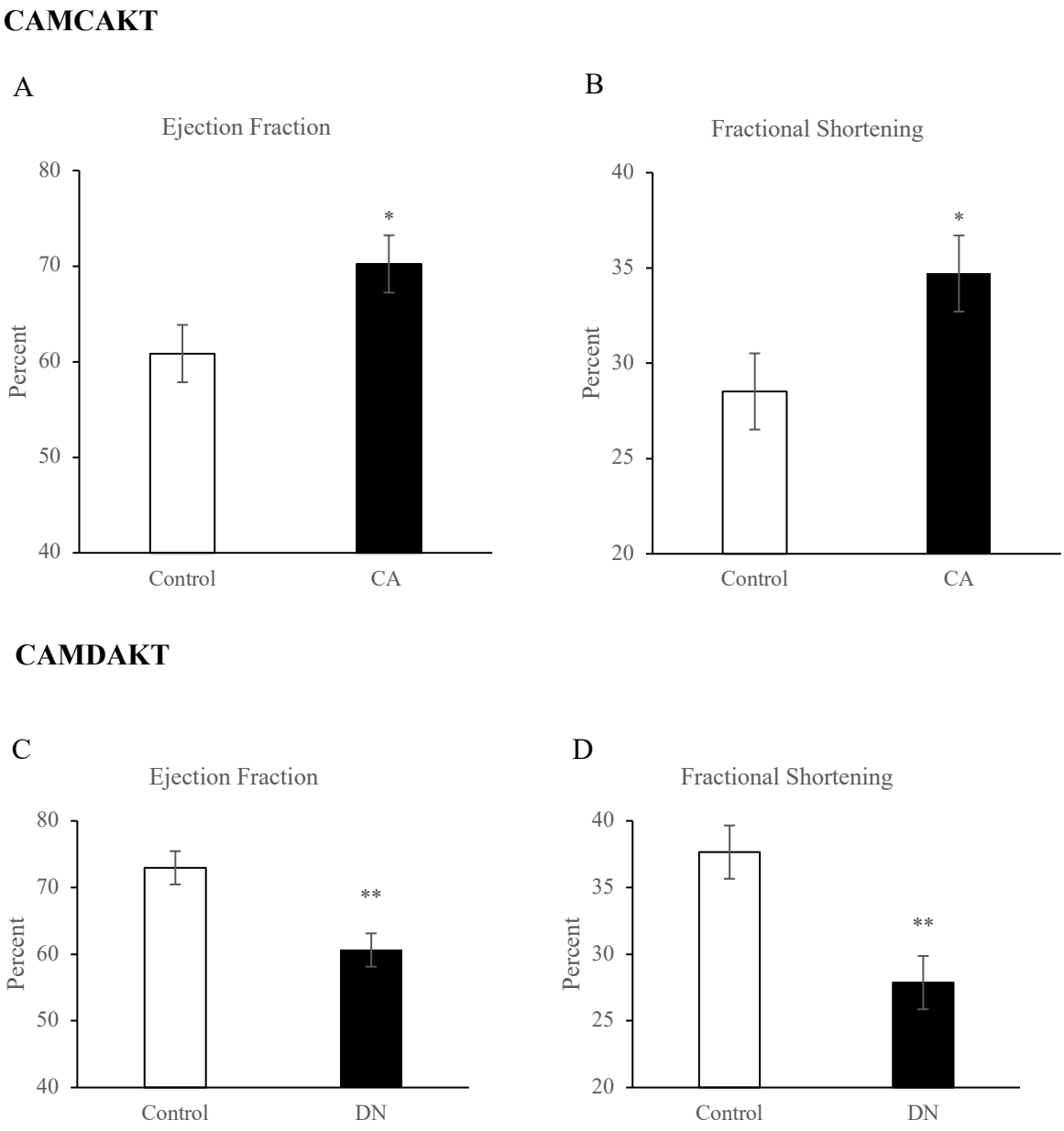

Figure 2.6 Mitochondrial Akt1 Protected Cardiac Function. Ejection fraction (A) and fractional shortening (B) are improved in CA mice compared on controls after 5 months of HFF (n = 6,8, *p < 0.05). Ejection fraction (C) and fractional shortening (D) are impaired after induction of DN mice compared to their respective controls (n = 14,15, **p < 0.01).

Figure 2.7

CAMCAKT

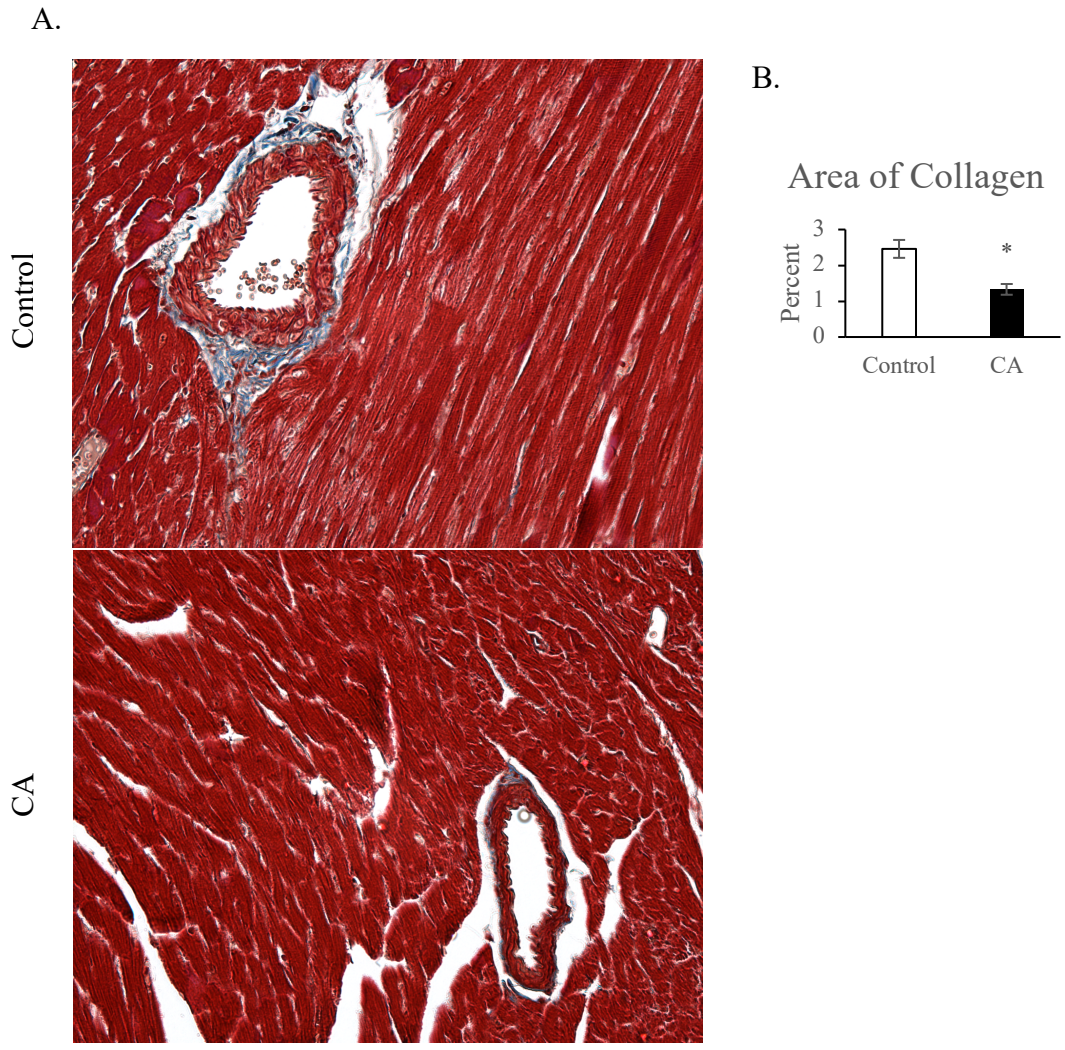

Figure 2.7 Constitutively Active mito-Akt1 Reduced Formation of Perivascular Fibrosis.

(A) CA mice exhibited less perivascular fibrosis after 5 months on a HFF compared to controls.

(B) Images were quantified ($n = 12$, $p < 0.05$).

Figure 2.8

CAMCAKT

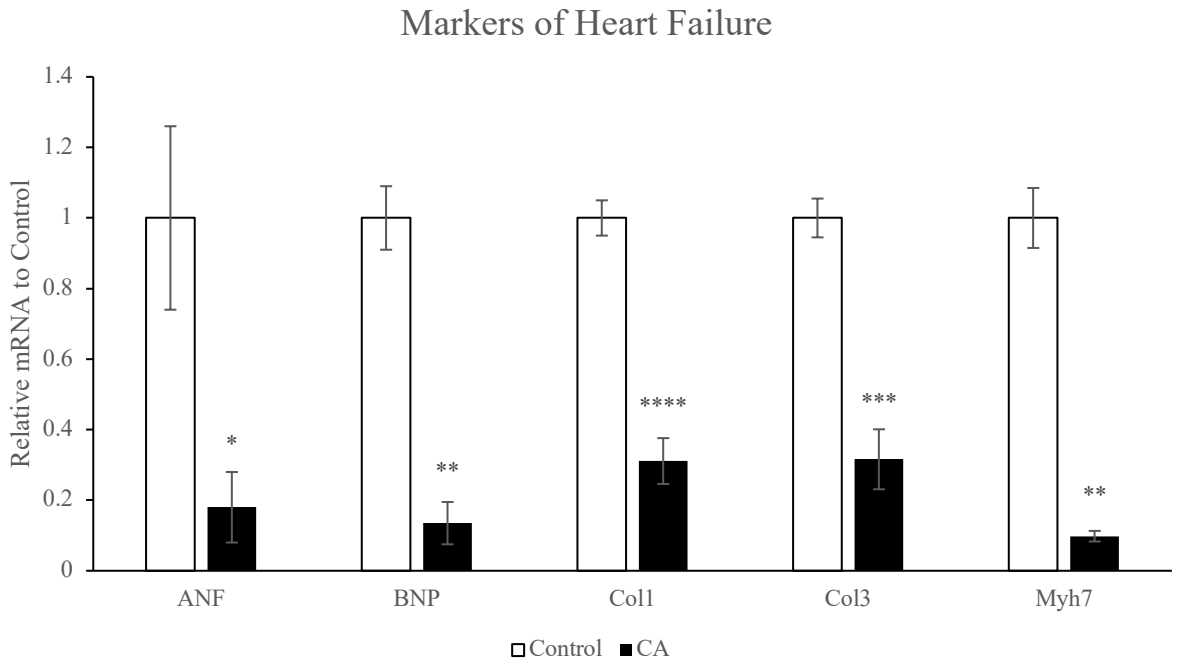

Figure 2.8 Constitutively Active mito-Akt1 Reduces Expression of Heart Failure Markers. CA mice had significantly lower expression of heart failure markers compared to controls after 5 months on HFF (n = 5,8, *p < 0.05, **p < 0.01, ***p < 0.001, ***p < 0.0001).

Figure 2.9

CAMCAKT

A.

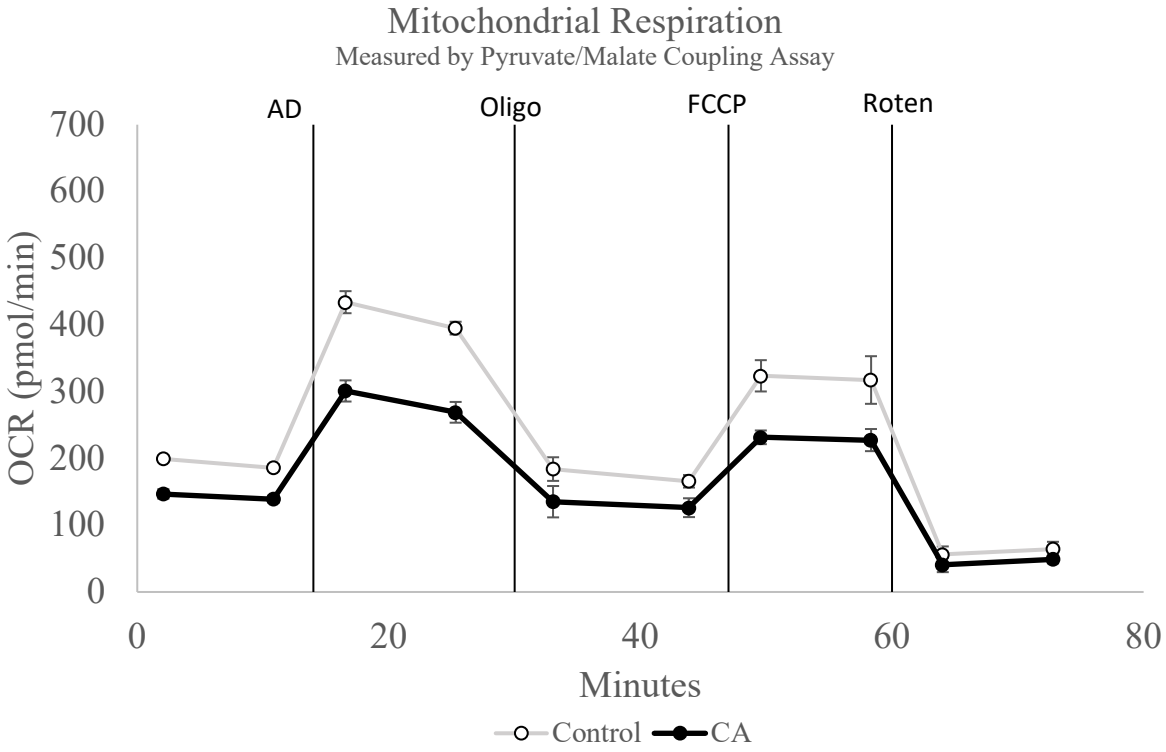

B.

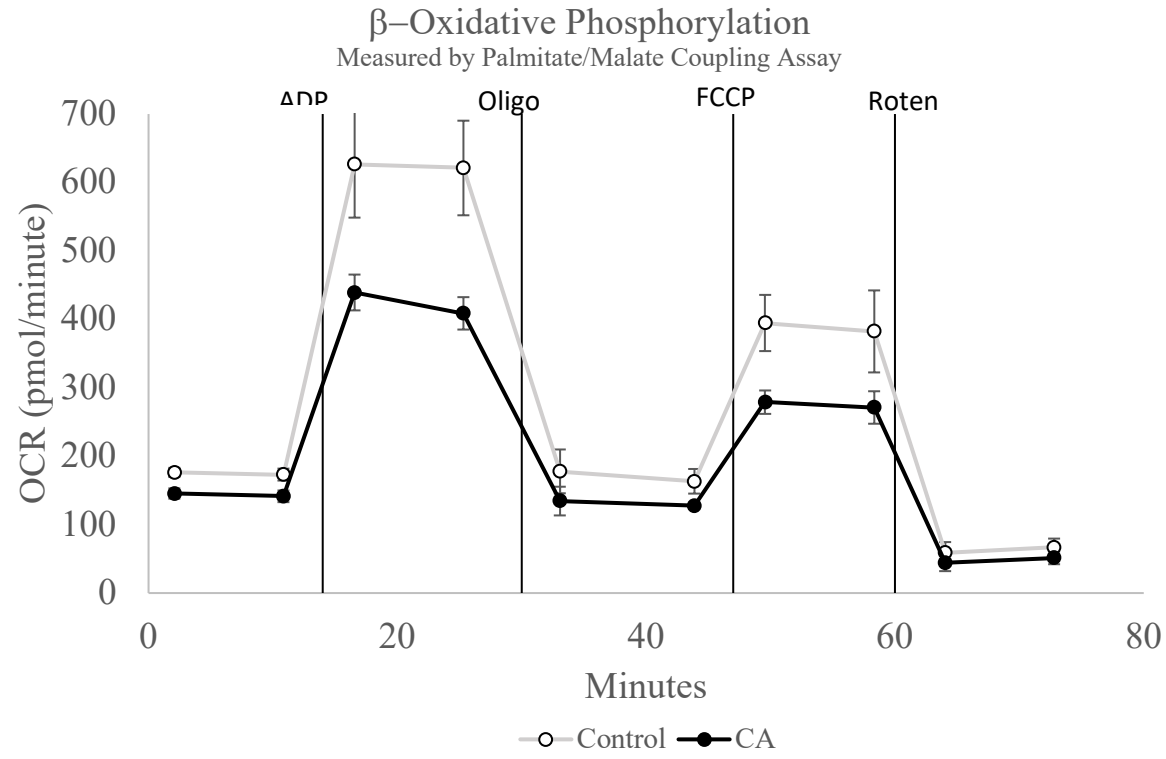

C

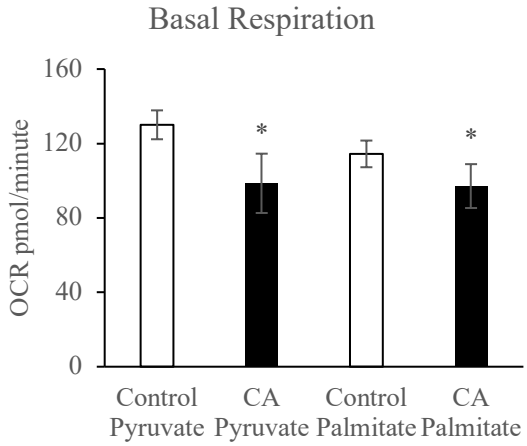
Basal Respiration
OCR pmol/minute
160
120
80
40
0
*
*
Control Pyruvate
CA Pyruvate
Control Palmitate
CA Palmitate

D

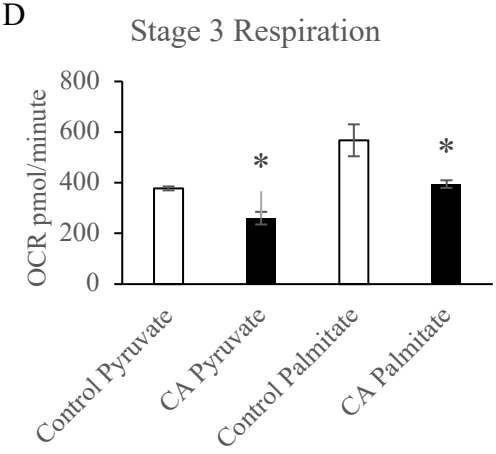
Stage 3 Respiration
OCR pmol/minute
800
600
400
200
0
*
*
Control Pyruvate
CA Pyruvate
Control Palmitate
CA Palmitate

E.

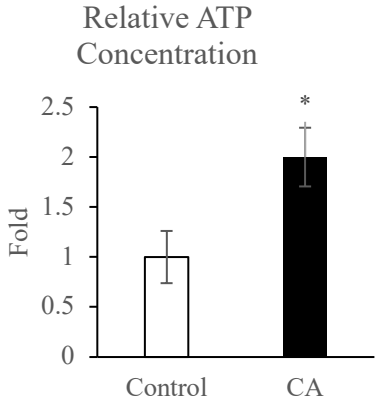
Relative ATP Concentration
Fold
2.5
2
1.5
1
0.5
0
*
Control
CA

F.

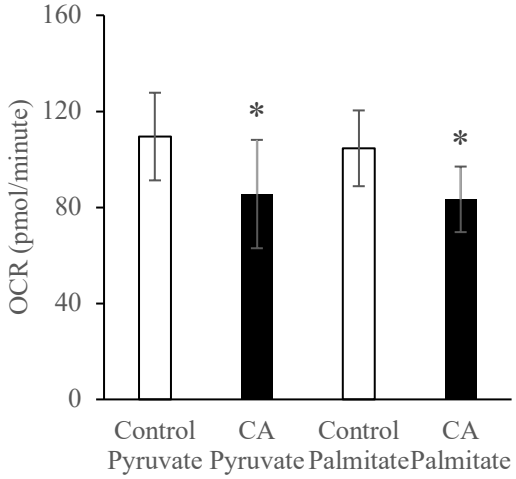
Proton Leak
OCR (pmol/minute)
160
120
80
40
0
*
*
Control Pyruvate
CA Pyruvate
Control Palmitate
CA Palmitate

Figure 2.9 Constitutively Active mito-Akt1 Improves Mitochondrial Respiration Efficiency. Pyruvate/Malate (A) and Palmitate/Malate (B) assays were carried out on isolated mitochondria from CA and control mice after 2 months on HFF. CA mice exhibited significantly lower oxygen consumption on both substrates. Basal respiration (C) and Stage 3 respiration (D) were significantly lower in CA mice while utilizing either pyruvate or palmitate. Mitochondria from CA mice contained markedly higher ATP concentration while maintaining lower levels of proton leak (E) ($n = 6$, $*p < 0.05$).

Figure 2.10

CAMCAKT

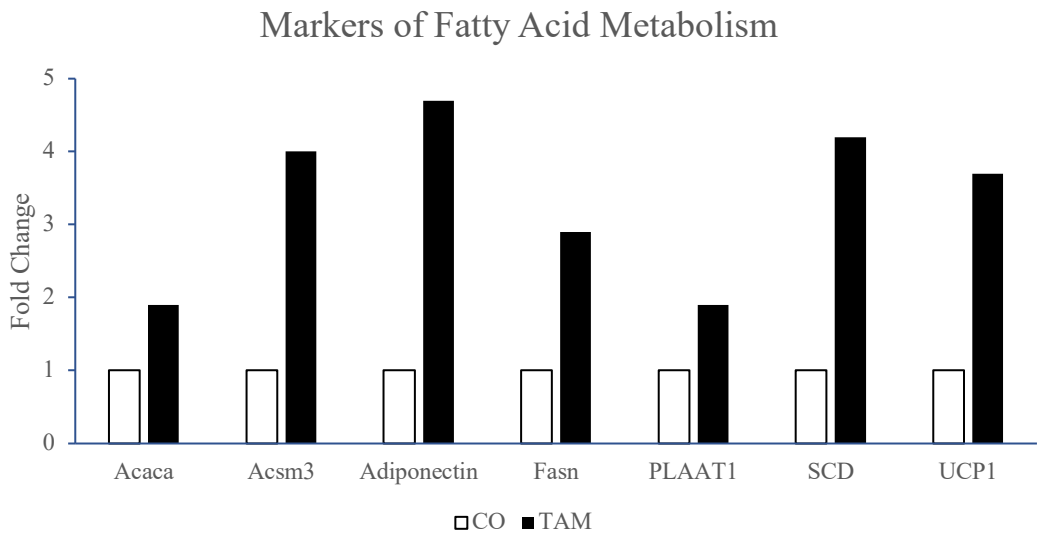

Figure 2.10 Marker of Fatty Acid Metabolism are Increased by Cardiac mito-Akt1 Signaling. Expression of marker genes of fatty acid metabolism were upregulated in CA myocardium. Acaca, Acsm3, Scd catalyze synthesis of acyl-CoA. Adiponectin, a protein hormone, promotes fatty acid synthesis. Phospholipase A hydrolyzes phospholipids into fatty acids. UCP1 consumes energy for thermogenesis.

CHAPTER 3

Cardiac Mitochondrial Akt1 Modulates Whole Body Metabolism

I. Introduction

Obesity is commonly associated with type 2 diabetes as their causes and pathologies are intertwined. In our diet-induced diabetes model, we previously established that maintaining heart mitochondria Akt1 signaling protects against cardiomyopathy, in part, due to promoting optimal metabolism. The heart consumes the most energy per mass of any organ in the body, and improving its functions yields metabolic benefits beyond myocardium.

II. Background

Obesity has been clinically classified as a having a body-mass index of 30 or higher, although more recent diagnoses take in account additional measurements. Chronic diseases such as obesity and diabetes have emerged as leading health concerns since the last turn of the century as management of infectious diseases improved [51]. The Behavioral Risk Factor Surveillance System (BRFSS), the National Health Interview Survey (NHIS), and the National Health and Nutrition Examination Survey (NHANES) have each documented dramatic increases in the prevalence of overweight and obesity since in the 1960s. Currently, nearly one third of those in the US are obese [52]. It is no longer a primarily adult disease as now, the CDC reports nearly 17% of children and adolescents suffering from obesity [53]. Several societal factors coincide to drive this new epidemic: a positive energy balance due to the greater availability and

consumption of food, decreased time spent in occupational and recreational physical activity, and [54] growing use of medications which have weight gain as a side effect .

A chronic positive energy balance leads to the accretion of lipids, primarily triglycerides, in adipose tissue, as well as skeletal muscle, liver, and other organs. An obese person will have a higher fat mass percentage, >25% in men and >33% in women. With weight gain over time, excess lipids are distributed to various body compartments with subcutaneous adipose tissue holding the majority of stored fat [55]. Over time, obesity drives the recruitment of macrophages and other immune cells to adipose tissue, in part, due to tissue remodeling in response to adipocyte apoptosis. Low grade systemic inflammation caused by immune cell secreted cytokines contributes to insulin resistance and is a major risk factor for type 2 diabetes [56].

Clinically, BMI is the most widely used metric for diagnosis, but recent data has shown that it may not be suitable for every case due variation in body types. Waist circumference, a useful measure of intraabdominal and upper-body subcutaneous adipose tissue should be considered as well as family history, psychiatric history, serum metabolites, and behavioral history [57]. Behavioral changes, including calorie restriction and increase physical activity, supported by therapy remains one of the most effective treatments for obesity [58]. Awareness, diagnosis, and lifestyle modifications are critically important as obesity is a major risk factor for both cardiovascular disease and type 2 diabetes.

III. Materials and Methods

1. Body Composition Measurement

Body composition was determined using an EchoMRI^{TM} 3-in-1 body composition analyzer (Echo Medical Systems, Houston, TX). Mice are individually placed in acrylic specimen holders

and compressed in place based on body size and placed into the EchoMRI^{TM} analyzer for a live reading. Analyzer was calibrated using a corn oil cartridge. Following the manufacturer's standard protocol, measurements of whole-body fat, lean mass, free water and total water, and total weight are taken. Calculation of body fat percentage is the reported as whole body fat divided by the total weight determined by the analyzer. Lean mass percent is reported as the lean mass divided by the total weight determined by the analyzer.

2. Metabolic Cage

Energy expenditure was evaluated using a TSE PhenoMaster System. Mice were placed in the metabolic cages for 7 days and provided with either normal chow and water or HFF diet depending on the prior cage conditions. Movement, CO2 production and O2 consumption were collected every 60 min for each mouse during the 7 days. The light cycle ran from 6 AM to 6 PM followed by a dark cycle. The levels were normalized to the lean mass. Reported measurements exclude the first two days in which the mice were acclimating to the metabolic cages, to reduce variability.

3. Oral Glucose Tolerance Test

For measuring glucose tolerance, mice were fasted for 6 hours, starting at 7 AM the day of the experiment. All food and corncob-based bedding were removed; water was provided. At the beginning of the experiment, the tail was clipped, and blood glucose was measured using a standard glucometer. All mice were given 2g glucose/kg body weight from a stock glucose solution of 0.5g/mL by oral gavage. The glucose stock solution was prepared the day before the experiment (Sigma #G6152). Blood glucose was measured at 15-, 30-, 60-, and 120-minute time

intervals after initial glucose gavage. Blood was collected by retro orbital bleeding for insulin concentration determination at each time point. Mice were sacrificed after oral glucose tolerance test. Blood samples collected were centrifuged at 10,000g for 10 minutes to remove blood cells; the upper serum fraction was stored. Insulin concentration at each time point was determined from serum samples using a Mouse Insulin ELISA Kit (Abcam, ab277390) according to the manufacturer's protocol.

4. Lipid Panel

Serum triglyceride was quantified using a Triglyceride Assay Kit (Abcam ab65336) accord to the manufacturer's protocol. To measure serum cholesterol, an HDL and LDL/VLDL Cholesterol Assay Kit (Abcam ab65390) was used according to the manufacturer's protocol. 8 uL of serum per sample were used for assays.

IV. Results

1. Cardiac mito-Akt1 Signaling Promotes a Leaner Body Composition.

Body composition was measured using an NMR-MRI based body analyzer. Output of fat mass, lean mass, and total water were recorded. Body fat percentage was calculated by dividing fat mass over total mass and lean mass percentage was calculated by dividing lean mass by total mass.

At 8 weeks old, before being placed on a HFF diet, all mice were lean, at 10% body fat (Figure 3.1A). Body composition measurements were taken after multiple durations of HFF feeding. Body fat percentage increased, as expected, until all mice reached a plateau at 40% (Figure 3.1A). Consistent with these measurements, the lean mass percent decreased accordingly

over the same period (Figure 3.1B). Interestingly, during the 1–2-month HFF diet duration window, there was a significant reduction in body fat in CA mice compared to controls ($n = 12$, $p < 0.05$) (Figure 3.1A). In male mice, CA mice had 15% less body fat – 5% lower body fat percent ($n = 12$, $p < 0.05$) (Figure 3.1C) and 9% greater lean mass – 5% greater lean mass ($n = 12$, $p < 0.05$) (Figure 3.1D) percent compared to controls after 2 months of HFF diet. In female mice, there was no difference in body composition between CA and controls (Figure 3.1E, F). This was our first indication that augmenting cardiac Akt1 signaling in our model may have effects beyond the heart and may indeed have beneficial effects at the whole-body level.

2. Cardiac mito-Akt1 Signaling Increases Energy Expenditure

Based on our body composition results, we wanted to further investigate the 2 month HFF diet duration time point as the differences in phenotype, and underlying molecular changes, may be the most prominent at this stage. Utilizing metabolic cages, mice were individually housed and monitored to track oxygen consumption, carbon dioxide production, temperature, movement, and other metrics. To improve consistency, mice were allowed two days to acclimate to the cages and the following four days of measurements would be averaged and used for calculations. A readout of the raw data, taken at 30-minute intervals, is provided (Figure 3.2 A,B) ($n = 8$). Note that dark periods, occurring from 6PM to 6AM are associated with higher activity.

To further analyze the results, data points were binned into dark and light periods with the first hour after each transition omitted. Mice activity was significantly distinct between these two cycles with transition time delay of roughly one hour. Male CA mice consumed 15% and 19% and more oxygen than controls during the day and night cycles respectively, normalized to

body weight ($n = 8$, $p < 0.05$) (Figure 3.2C). The same mice produced 17% and 20% and more carbon dioxide than controls during respective day and night cycles ($n = 8$, $p < 0.05$) (Figure 3.2D). From these data, total energy expenditure was derived. Male CA mice expended 13% and 12% more energy, normalized to body weight, compared to controls during the day and night cycles respectively ($n = 8$, $p < 0.05$) (Figure 3.2E). Female mice were also measured, and CA mice found to expend 17% and 21% more energy than controls over the same day and night cycles ($n = 8$, $p < 0.05$) (Figure 3.2F). Notably, the respiratory exchange ratio was unchanged suggesting no significant switch in energy substrate overall ($n = 8$, $p < 0.05$) (Figure 3.2G). Together, these results indicate that cardiac mitochondrial Akt1 signaling results in increases in metabolism so profound that it was detectable at the whole organism level.

3. Glucose Tolerance and Insulin Sensitivity were Unchanged by Cardiac mito-Akt1 Signaling

Glucose tolerance was measured using an oral glucose tolerance test, during which time, blood was drawn to determine serum insulin concentration. No difference in glucose tolerance was measured in either gender mice at 2 months on the HFF diet (Figure 3.3A, B). Nor was a change detected after 5 months on a HFF diet. Insulin levels were also unchanged in both genders (Figure 3.3 C, D). As expected, female fasting blood glucose levels were lower than male levels, as was insulin levels. (Figure 3.3). Although not significant, CA fasting glucose and insulin may trend lower than their controls. Cardiac mitochondrial Akt1 did have an apparent effect on insulin sensitivity nor glucose tolerance.

4. Cardiac mito-Akt1 Signaling Lowered Serum Cholesterol Levels

Serum cholesterol and triglyceride levels were measured. While triglyceride levels were unchanged (Figure 3.4A), serum cholesterol was significantly lower in CA mice after 2 months of HFF diet. Total cholesterol was 34% lower while LDL levels were 41% lower ($n = 4$, $p < 0.05$) (Figure 3.4B). Activation of cardiac mito-Akt1 was able to reduce serum levels of LDL and consequently, total cholesterol.

V. Discussion

With this set of experiments, we demonstrated the massive bioenergetic impact that the heart has on the entire body. It is unsurprising, given the high energy consumption, but the results are striking.

Our diet induced diabetes model effectively generated a phenotype of obesity. As early as three months of being on a high fat and fructose diet, the mice reached nearly 40% percent body fat. By comparison, greater than 25% body fat is considered obese in humans. Interestingly, CA mice were leaner than their control counterparts in the early stages, but beyond 2 months of the HFF diet, this difference was diminished and both groups reached a plateau of adiposity. Considering that we only directly modulated cardiac signaling, our data suggests that, while the heart maintained optimal function throughout the study period, its metabolic contribution becomes proportionally reduced as weight gain and fat accumulation increases. We also observed a gender difference in that females did not exhibit a difference in body composition between CA and control animals. Although, female mice are significantly leaner overall than male mice while on the same diet and therefore, possible cardiac effects may be less detectable.

Based on these results, we selected a 2-month HFF diet study design to further interrogate metabolic changes in the body, promoted by the heart. At this interval, diabetes and other

phenotypes of metabolic syndrome have developed but have not yet progressed to a severity that would obfuscate changes brought about by cardiac mitochondrial Akt1 signaling. Reduced adiposity has wide ranging benefits. In particular, reduced adiposity reduces inflammatory cytokines and improves insulin sensitivity, reduces the release of free fatty acids by adipose tissue and reduces dyslipidemia [59].

To understand the body composition changes, we tracked the metabolic activity CAMCAKT mice individually after 2 months of being on a HFF diet. Over the measurement period, we were able to determine that indeed, CA mice expended more energy than their control counterparts. Energy expenditure was derived using precise oxygen consumption and carbon dioxide production measurements. Here we did observe the same proportion of increase in energy expenditure in both genders although it should be noted that basal energy expenditure is significantly higher than in males, when normalized to body weight. Increased whole body energy usage explains the increase in leanness of male CA mice. In female mice, because percent body fat was far lower, differences in energy expenditure may not have yielded a measurable difference in body composition.

The increase in oxygen consumption measured by metabolic cage and decrease measured by extracellular flux assay may seem contradictory but the different conditions should be clarified. While the metabolic cage was an assay of oxygen consumption at a whole animal level, the extracellular flux assay was measuring the maximal potential respiration of a normalized quantity of mitochondria under fuel saturating conditions. Put in context, our data suggested that CA mice exerted more energy in vivo while simultaneously, at the molecular level, metabolizing energy substrates at a higher respirational efficiency.

In our model, fasting glucose and insulin levels were not significantly changed. Although fasting glucose and insulin levels may have trended lower, but we are not yet certain without further investigation. The increased leanness may have afforded a greater degree of insulin sensitivity [59]. Serum levels of cholesterol, particularly LDL, were lowered in CA mice, potentially due to the greater fatty acid metabolism of the heart and also due to increased insulin sensitivity [60].

In these series of experiments, we showed the substantial effects cardiac metabolism can have at the whole-body level. Improved heart energy consumption was measurable in vivo and even increased body leanness. Reduced adiposity has well documented benefits in improving insulin sensitivity and reduced serum fatty acid content. Aside from being an energy sink, the heart's role as an inter-organ regulator is emerging field of research. We asked further, if cardiac mitochondrial Akt1 signaling may alter the heart's regulatory role, particularly on other organs with high energy demands, such as the liver.

VI. Figures

Figure 3.1

CAMCAKT

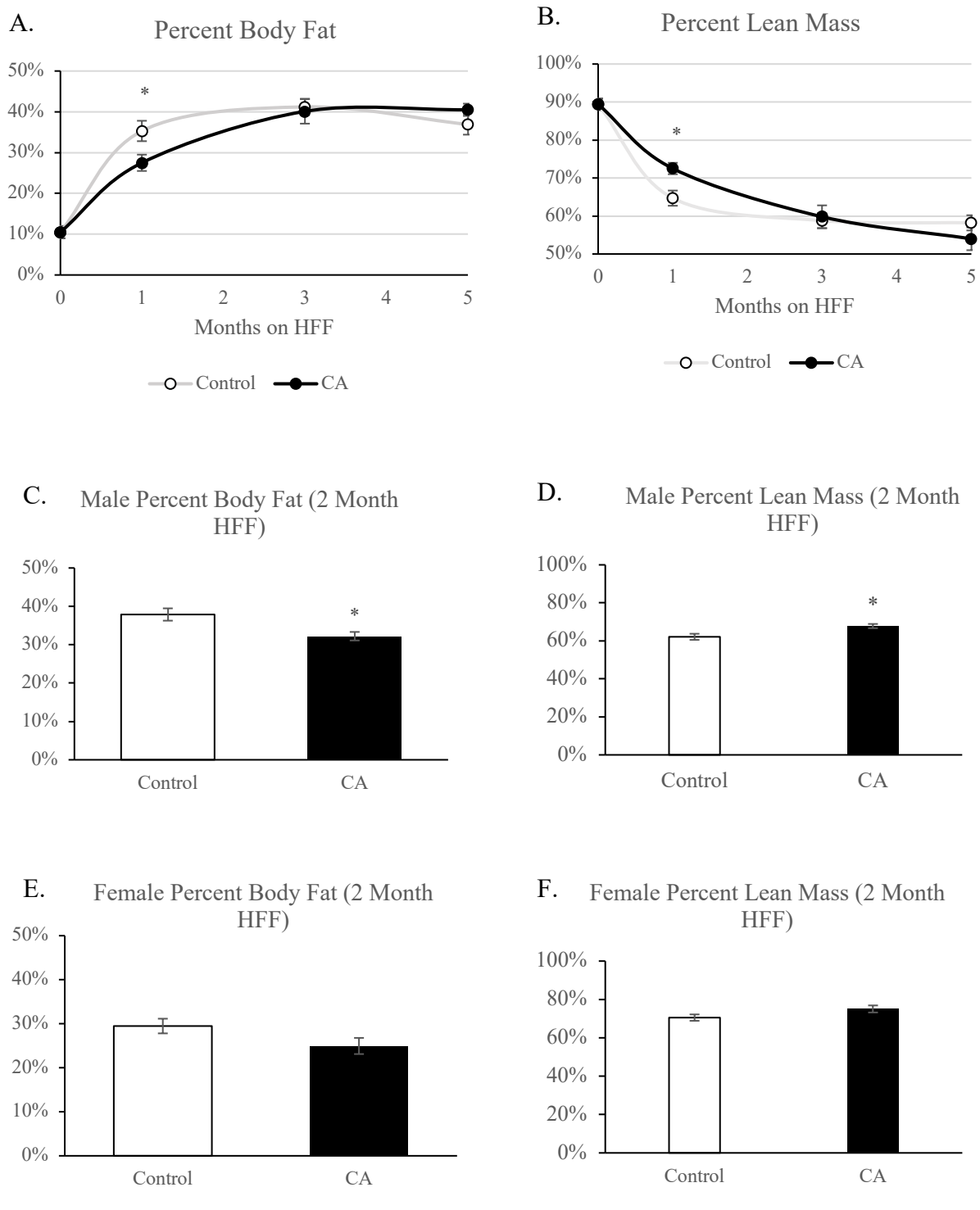

Figure 3.1 Cardiac mito-Akt1 Signaling Promotes a Leaner Body Composition. Body composition measurements of percent fat mass (A) and lean mass (B) of CA and control mice over time on HFF are presented. Male CA mice are leaner than controls 1-2 months into the HFF diet (C), (D), while no difference was measured in female mice (E), (F) ($n = 12$, $*p < 0.05$).

Figure 3.2

CAMCAKT

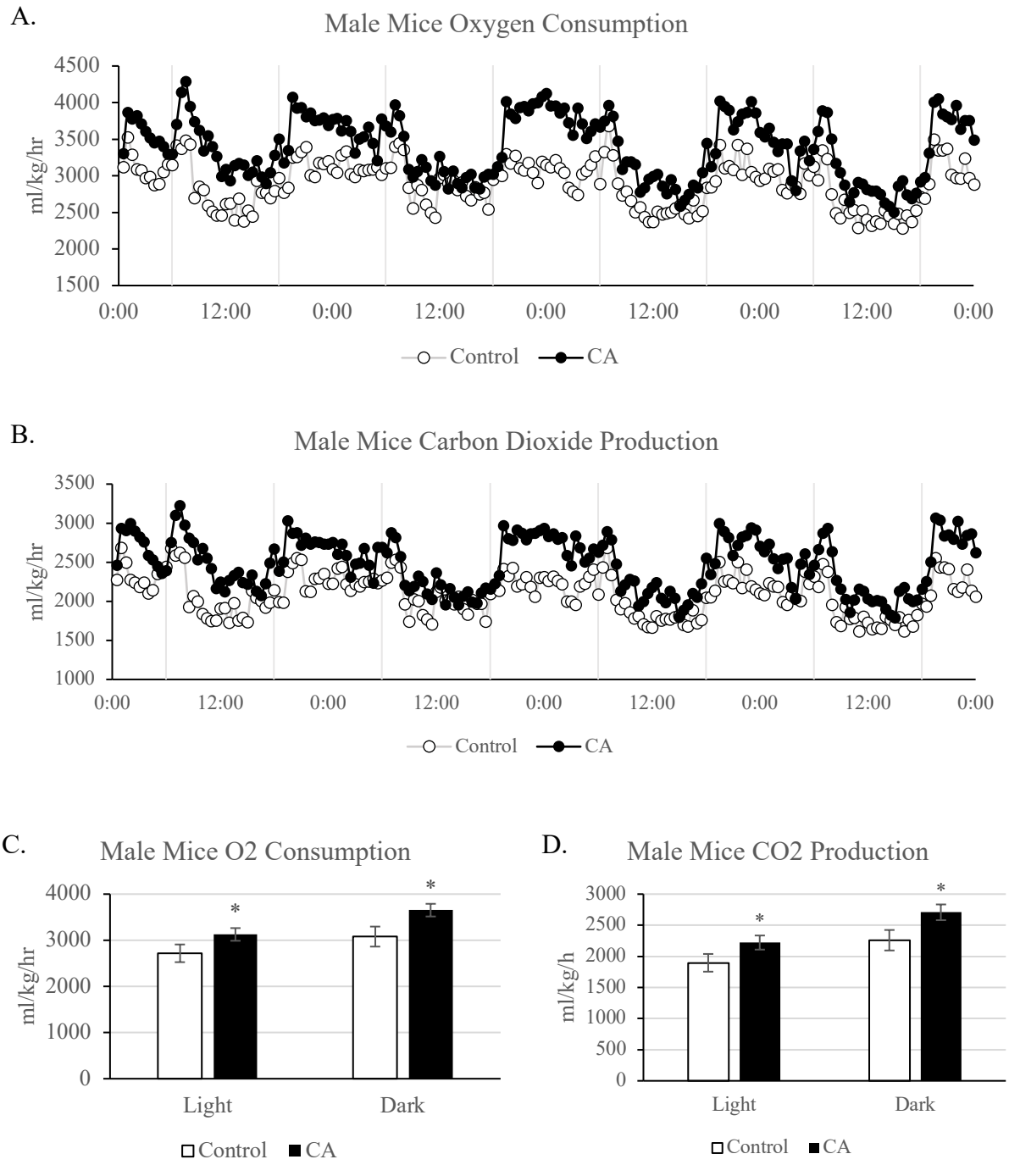

E.

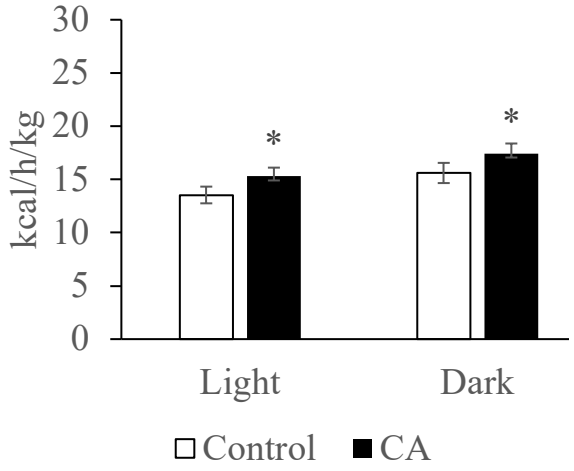
Male Mice Energy Expenditure
kcal/h/kg
30
25
20
15
10
5
0
*
*
Light
Dark
Control
CA

F.

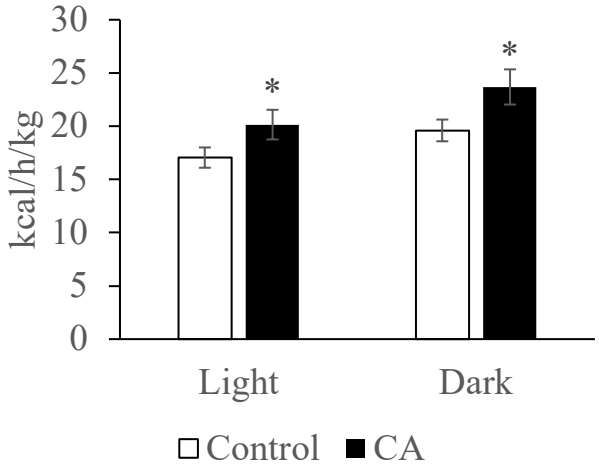
Female Energy Expenditure
kcal/h/kg
30
25
20
15
10
5
0
*
*
Light
Dark
Control
CA

G.

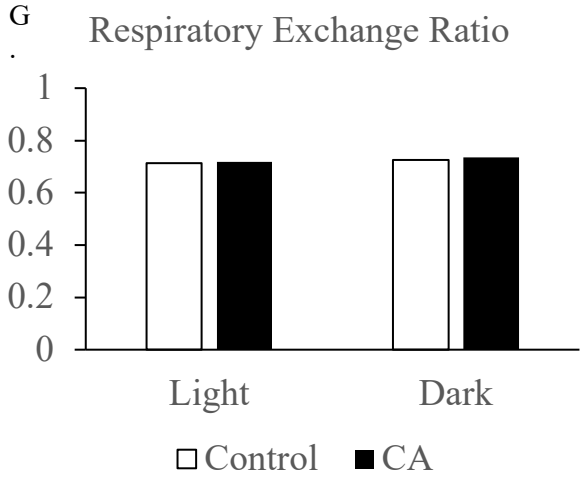
Respiratory Exchange Ratio
1
0.8
0.6
0.4
0.2
0
Light
Dark
Control
CA

Figure 3.2 Cardiac mito-Akt1 Signaling Increases Whole Body Energy Expenditure. Oxygen consumption (A) and carbon dioxide production of individual mice are shown over the course of four days. Measurements, combined into light (C) and dark cycles (D), show that CA mice had higher oxygen consumption and carbon dioxide production during both periods of the day compared to control mice, after 2 months HFF. Energy expenditure was increased in both male (E) and female (F) mice while the respiratory exchange ratio remained unchanged by cardiac mito-Akt1 signaling ($n = 8$, $*p < 0.05$).

Figure 3.3

CAMCAKT

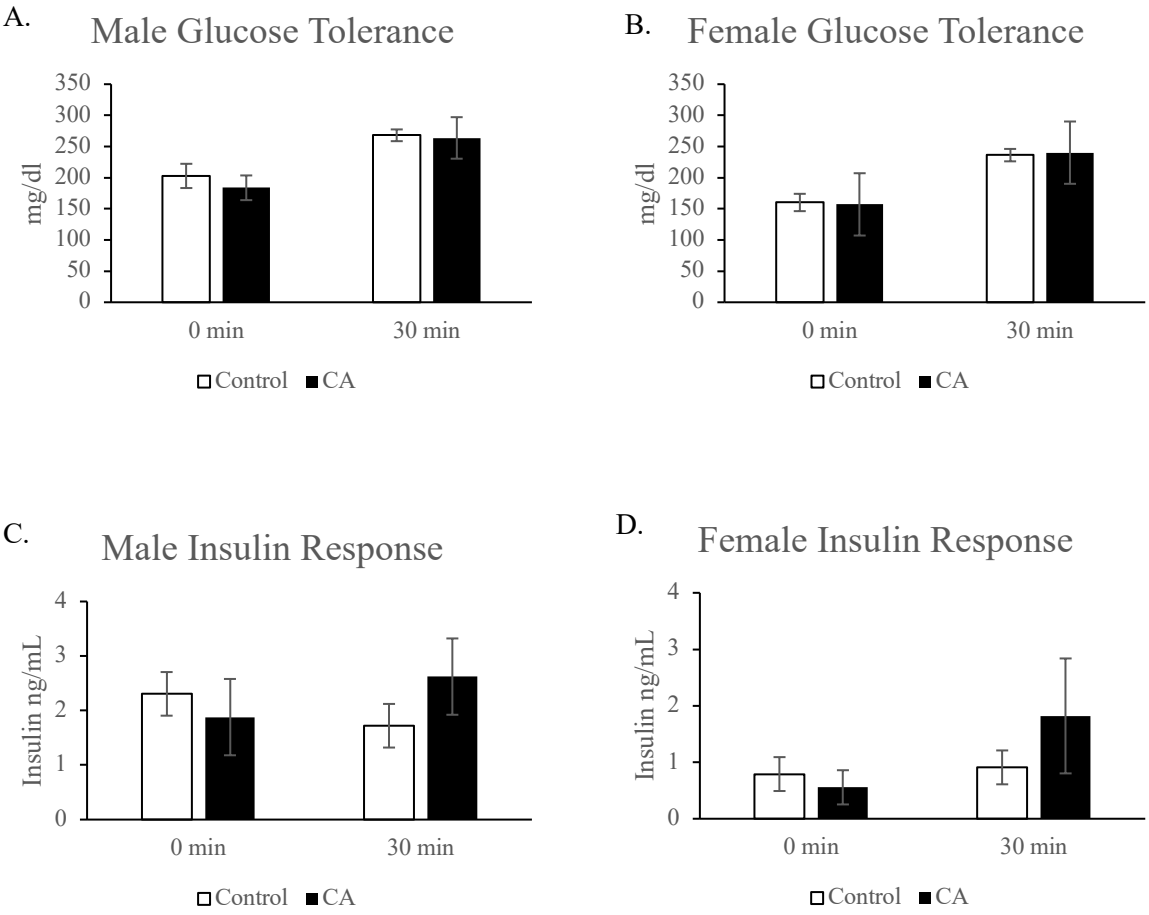

Figure 3.3 Glucose Tolerance and Insulin Sensitivity were Unchanged by Cardiac mito-Akt1 Signaling. No difference in oral glucose tolerance (A), (B) nor serum insulin measurements (C), (D) were exhibited by either male or female CA mice (n = 8).

Figure 3.4

CAMCAKT

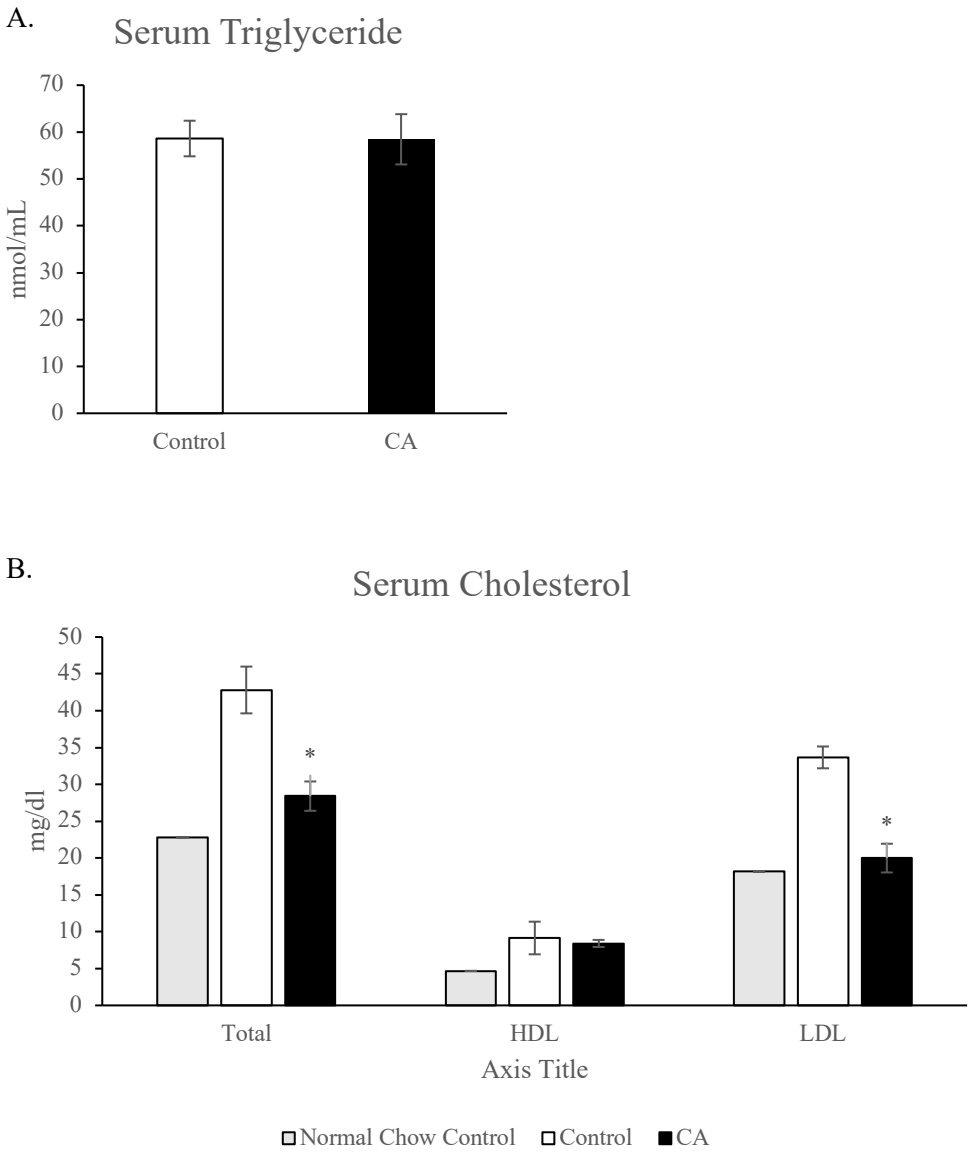

Figure 3.4 Cardiac mito-Akt1 Signaling Altered Serum Cholesterol Levels. While total serum triglyceride levels were unchanged (A), total cholesterol and LDL levels (B) were lowered in CA mice after 2 months on HFF ($n = 6$, $*p < 0.05$).

CHAPTER 4

Cardiac Mitochondrial Akt1 Signaling Attenuates NAFLD

I. Introduction

The liver is metabolic organ with the high energy demands, second only to the heart, normalized by mass. Non-alcoholic fatty liver disease is closely associated with diabetes and, in turn, may be correlated to cardiomyopathy. Non-alcoholic fatty liver disease (NAFLD) is defined by macrovesicular steatosis in greater than 5% of hepatocytes independent of a secondary cause such as alcohol or drug consumption [61]. NAFLD encompasses the whole spectrum of liver steatosis diseases from non-alcoholic fatty liver (NAFL) to non-alcoholic steatohepatitis, fibrosis, and cirrhosis. The complex cardiohepatic interactions involved are not yet well understood. We set out to characterize the interactions between cardiac mito-Akt1 signaling and hepatic metabolism and make data modeling-based predictions about the mechanisms of heart and liver crosstalk in our model.

II. Background

NAFLD has become the leading cause of chronic liver disease and is the leading cause of cirrhosis requiring liver transplant [62]. Worldwide, the prevalence of NAFLD is 25%, up from 15% in 2005. There is a close association with type 2 diabetes with 23% of diabetic patients also suffering from NAFLD, as well as close associations with central obesity, dyslipidemia, and metabolic syndrome [63]. A small percentage of patients suffering NAFLD will develop complications of chronic liver disease, with up to 5% dying from hepatocellular carcinoma and

up to 8% from cirrhosis. However, the number of patients suffering from end stage NAFLD is rapidly increasing with cases rising 170% in the decade spanning 2004 to 2013 in the United States [64].

1. Pathogenesis

Insulin resistance in the liver is implicated as one of the main drivers of NAFLD. The accumulation of triacylglycerol (TAG) within the liver comes from three sources: dietary lipids, adipose-derived fatty acids, and de novo-synthesized fatty acids within the liver [65]. Free fatty acids entering portal circulation are processed in one of three ways: β-oxidation, re-esterification to TAGs and exported as very low-density lipoprotein (VLDL), or re-esterification for storage in the liver. De-novo synthesis of lipid (DNL) from carbohydrates is increased in states of hyperinsulinemia such as insulin resistance [66]. In addition, gluconeogenesis is increased in individuals with NAFLD, adding an additional substrate source for DNL [67].

As NAFLD progresses, about 23% of cases progress to non-alcoholic steatohepatitis (NASH)- inflammation of the liver due to fat accumulation [68]. The exact mechanisms leading to development of steatohepatitis from simple fatty liver disease are still unclear. Currently, the proposed theory of the development of NASH is multiparallel hypothesis of several conditions acting simultaneously [69]. Genetic predisposition, altered lipid metabolism, oxidative stress, mitochondrial dysfunction, lipotoxicity, altered cytokine and adipokine production may all be contributing factors.

Inflammation is a key factor of NASH pathogenesis. Driving inflammation is elevated levels of toxic lipids which increase cellular stress and induce pro-apoptotic signaling [70]. TNF-related apoptosis-inducing ligand (TRAIL-R), Fas and tumor necrosis factor receptor (TNFR) are

upregulated in NASH indicating that they may have a role in inflammation promotion and chemokine secretion [71]. Kupffer Cell activation is critical in NASH development and proceeds the recruitment of other immune cells. Kupffer cells are activated both by hepatic toxic lipids and well as interaction with toll-like receptors on damaged hepatocytes. Subsequently, secretion of pro-inflammatory cytokines: IL-1β, IL-12, TNF-α, CCL2 and CCL5 are induced, further causing hepatocyte damage [72]. A positive feedback loop then results as damaged hepatocytes express damage-associated molecular patterns, further activating immune cells [73]. Dendritic cells and Natural Killer cells are also recruited but have both inflammatory and anti-inflammatory roles within the liver and thus, their contribution to NASH pathogenesis is still unclear [74, 75].

The progression of NAFLD to end stage liver disease, most notably, cirrhosis, or severe irreversible scaring of the liver tissue, varies depending on the underlying histology. NAFLD patients with simple steatosis have a 4% chance of developing cirrhosis while those with NASH have up to a 25% chance of their condition progressing to cirrhosis [76]. Once cirrhosis reaches the point of liver decompensation, or acute liver failure, the median survival time is approximately 2 years [77].

2. Diagnosis

Clinical investigation of NAFLD is typically only initiated following detection of elevated liver transaminases. However, patients with Type 2 diabetes are also recommended to be examined for NAFLD due to the high associated risks [78]. Until recently, ultrasound examination has been the de facto diagnostic modality due to its high accessibility but is limited in its sensitivity for detection of low-level steatosis [79]. Newer technologies such as transient elastography can be used to measure both liver steatosis and fibrosis [80]. Multiple serological

tests are also available which identify levels of markers including fibroblast growth factor 21 (FGF21), aspartate transaminase (AST), alanine transaminase (ALT), cytokeratin 18 (CK18) and others [81].

3. Management

There are currently no medications currently approved for the direct treatment of NAFLD although some traditional treatments for diabetes have shown mild benefits. Metformin has been demonstrated to lower body fat and improve hepatic insulin sensitivity by suppressing hepatic gluconeogenesis [82]. Thiazolidinediones, a PPARγ ligand, prescribed to type 2 diabetic patients, have been shown to improve insulin sensitivity in adipose tissue, increasing its lipid uptake and storage, thus redirecting fatty acids from liver uptake [83]. Other therapeutics, such as glucagon-like peptide-1 (GLP1) analog therapies may also improve liver steatosis, but the mechanism is unclear. Many existing therapies may function to attenuate liver steatosis indirectly by promoting weight loss [84].

One of the most clinically effective means of preventing and even reversing liver steatosis is lifestyle modification through reducing caloric intake and increasing physical exercise. In a clinical study, 50% of participants who lost at least 10% of their body weight exhibited regression in hepatic fibrosis, demonstrating the liver's capacity to heal [85]. Hepatic fibrosis has been shown to be reversible if actions are taken before severe scarring, or cirrhosis, occurs.

III. Materials and Methods

1. Liver Steatosis Quantification

Liver tissue sections were prepared, and HE stained as previously described. 10 images at 20x were captured by random sampling with a Zeiss AxioPlan2 microscope. Each image was then processed by ImageJ to determine the degree of steatosis. White areas were quantified using the color threshold function in ImageJ. White pixels were counted by setting the following threshold settings: Hue (0, 255), Saturation (0, 30) and Brightness (0, 255). Pixels under threshold were measured and considered total area of lipid droplet. The area of lipid droplets is then divided by total captured area giving a percentage of steatosis coverage.

2. RNA Isolation

30-50ug of tissue was used per sample for RNA isolation. Tissue sample was rinsed in PBS and homogenized in 700uL Trizol using a plastic microfuge tube pestle. Samples were incubated at room temperature for 5 minutes before adding 200uL chloroform and vortexed. After, samples were incubated for 3 minutes at room temperature before centrifugation at 12000g for 15 minutes at 4°C. The resultant top aqueous layer was transferred to a new tube and 500uL isopropanol added, mixed and incubated at room temperature for 10 minutes. After, samples were centrifuged at 12000g for 15 minutes at 4°C. The resulting pellet was washed with 500uL ice cold 80% ethanol and then centrifuged again at 10,000g for 10 minutes at 4°C. Supernatant was discarded, pellet was dried for 5 minutes and then resuspended in 20-50uL DEPC water.

3. RNA Sequencing

RNA sequencing was performed by the UC Irvine Genomics High Throughput Facility. RNA was isolated from heart and liver tissue as previously described. Each sample submitted for sequencing was prepared by pooling equal RNA amounts from three mice of the same

experimental conditions. RNA sequence was performed on an Illumina NovaSeq6000 on an S1 flow cell. 12 samples were run on each lane resulting in a read depth of more than 60 million. Reads were analyzed by CLC Genomics Workbench 20.0 (Qiagen).

4. Quantitative Endocrine Network Interaction Estimation

(QENIE) analysis was performed by Dr. Marcus M Seldon at the University of California, Irvine. RNA sequencing data from heart and liver tissue of CA and control mice were provided as input. To identify secreted endocrine factors, correlations were screened for by examining global transcript levels between pairs of tissues and filtering for origin-tissue secretion based on expression arrays and RNA-seq data that constituted the Hybrid Mouse Diversity panel (HMDP) were utilized. Only proteins secreted by the target organ as annotated by the Universal Protein Resource (UniProt) database were included. The strength of cross-tissue predictions for endocrine circuits was termed S_{sec}

IV. Results

1. Cardiac mito-Akt1 Signaling Attenuates Liver Steatosis

Liver steatosis was quantified by image analysis of HE stained sections. Representative images of sections from CA and control liver after 5 months on HFF diet are shown (Figure 4.1A). Liver steatosis was measured after multiple durations on the HFF diet and as expected, lipid accumulation in the liver was progressively more severe, the longer the duration. A healthy liver should exhibit little to no steatosis. All mice at 8 weeks old, began with 5% steatosis by percent area of lipid droplet. After only 1 month, there was a dramatic difference in lipid accumulation, with livers from CA mice having a 50% perfect reduction in steatosis compared to

controls. Livers from CA mice had consistently less lipid accumulation, even up until 5 months where there was still a 21% reduction ($n = 12$, $p < 0.05$) (Figure 4.1B).

The two-month HFF diet duration continued to be a time point of interest for us as the CA liver exhibited significantly less steatosis than controls (Figure 4.2A). Percent area of lipid droplets continued to be 50% less in CA mice (Figure 4.2B) and additionally, average droplet size remained to be 50% smaller as well ($n = 12$, $p < 0.05$) (Figure 4.2C). These data clearly show that cardiac mito-Akt1 signaling attenuated liver steatosis.

2. Cardiac mito-Akt1 Signaling Reduced Markers of NAFLD

RNA sequencing analysis of liver tissue revealed several indicators of NAFLD were reduced. Collagen isoforms 16, 4, and 6 were reduced, indicating less severe fibrosis ($n = 6$, $p < 0.05$) (Figure 4.3). Matrix metalloproteinases 2 and 9 were downregulated as well as tissue inhibitor of matrix metalloproteinases 1, suggesting reduced activity of stellate cells depositing collagen into the liver extracellular matrix ($n = 6$, $p < 0.05$) (Figure 4.3). Hla-Dmb, Dqa1, and Dqb1 – MHC class 2 molecules, whose expression positively correlates with $CD4^+$ T cell infiltration was decreased ($n = 6$, $p < 0.05$) (Figure 4.3). Together, these markers indicate that NAFLD was reduced in CA mouse livers.

3. Cardiac mito-Akt1 Signaling Remotely Modulates Liver Metabolism Through Secreted Proteins

Quantitative Endocrine Network Interaction Estimation (QENIE) was performed by collaborator Dr. Marcus Seldon, University of California, Irvine, to identify heart secreted proteins which regulate liver function, based on RNASeq data sets on CA heart and liver

samples. Candidate proteins are listed in order of S_{sec} score, a predicted value of cross-tissue strength, or alternatively, the strength of their regulatory impact on predicted gene targets in the liver (Figure 4.4). Secretion of these candidate proteins were predicted to be upregulated in CA hearts and have corresponding effects on the liver.

4. Cardiac mito-Akt1 Signaling Promotes Myocardial Secreted Proteins Regulating Whole Body Metabolism

QENIE analysis of heart secreted proteins, upregulated by cardiac mito-Akt1, using HMDP clinical trait data, revealed whole body metabolism modulators. In addition, to altering gene expression profiles in the liver, some of the identified secreted proteins have known, correlated clinical outcomes. Proteins with positive and negative correlation are shown, colored by strength of correlated outcomes (Figure 4.5). Signaling peptides that regulated the liver also modulated glucose, insulin, serum lipids, body composition and body weight.

V. Discussion

In our model, we consistently saw reduced steatosis in CA mice compared to controls up to five months on the HFF diet, our longest study duration. This occurred despite the fact that differences in whole body adiposity diminished as the duration of the HFF diet increased. These data thus indicated that metabolism in the heart and liver here may be more closely and specifically interconnected. These set of experiments and RNA expression analysis aimed to characterize liver health as well as predict heart regulators which may modulate liver function.

CA mice clearly exhibited healthier livers. Histological analysis of livers from CA mice clearly showed reduced steatosis. Further analysis of the liver RNA expression data is consistent

with attenuated fatty liver disease. Several collagen isoforms were downregulated, an indicator of reduced fibrosis, a key feature of NAFLD. In addition, reduced markers of matrix metalloproteinases and antigen presenting molecules combined suggested reduced hepatic fibrosis and inflammation.

In a healthy liver, homeostasis of the extracellular matrix is maintained by continuous turnover of proteins, tightly regulation of matrix metalloproteinases (MMPs) and MMP inhibitors (TIMPs) [86]. Chronic damage of liver tissue prompts activation of hepatic stellate cells to differentiate into a fibroblast like phenotype, upregulating the expression of TIMP-1 and perturbing normal MMP activity. This leads to subsequent accumulation of matrix proteins in the extracellular space [86]. MMP-2 and MMP-9 were both found to be down downregulated in CA mice livers. Both deposit collagen as well as gelatin [87]. MMP-2 is expressed by HSCs during activation following liver injury, and further promoted by the presence of type 1 collagen [88, 89]. In animal models, MMP-2 RNA is hardly detectable in healthy liver tissue but expression is enhanced by CCl_4 induced fibrogenesis, stimulated by TGF-β and ROS [90]. MMP-9 is upregulated by IL-1b and TNF-α stimulated hepatocytes and, experimentally, by CCl_4 induced liver injury [91, 92]. TIMP-1 protein, on the other hand, regulates ECM composition by inhibiting active MMPs binding collagen to prevent its degradation [86]. Animal models and human studies have confirmed TIMP-1 upregulation due to inflammatory cytokines triggered by liver disease and found to be downregulated in CA mice livers [93, 94].

Infiltration of immune cells increases as NAFLD develops and is characteristic of NASH. HLA Class II molecules are expressed by antigen presenting cells such as dendritic cells and macrophages and are recognized by $CD4^+$ T cells [95]. In our model, HLA-DMB, HLA-DQA1, and HLA-DQB1 were downregulated in CA mice livers, indicating decreased T cell activation.

Hepatic expression if Class II antigens correlates well with the severity of liver injury and was attenuated by mito-Akt1 [96].

There is increasing evidence of cardiac control of the metabolism of peripheral organs and our model is further proof of this concept. The heart requires a substantial amount of energy and must dynamically adapt to changing demands. Current research is being done on studying heart-driven metabolic networks that coordinate peripheral organs. The heart may signal peripheral organs to reduce oxygen and nutrient consumption during periods of high demand while releasing energy substrates [97]. Recent clinical findings suggest that metabolic perturbations in the heart due to familial hypertrophic cardiomyopathy adversely impacts liver metabolism in part due to reduced lipid clearance from the blood by the heart [97]. The resultant increased left ventricular wall stress and pulmonary pressure is transmitted to the liver and causes hepatic congestion and alters the fatty acid profile of the liver. The consequent hepatic dysfunction in turn, aggravates cardiac dysfunction, demonstrating a feedback loop of cardiohepatic regulation.

More than 16 proteins secreted from the heart have thus far been classified as cardiokines, or endocrine peptides that allow for inter-organ and inter-cellular communication [97]. The earliest characterized chemokines were natriuretic peptides: ANF and BNP, released by failing hearts to decrease hemodynamic pressure, and shown to attenuate glycolysis in rat livers [97]. More recently, peptide Med13 was found to act through nuclear hormone receptors and shown to regulate systemic energy homeostasis. Specifically, Med13 increases lipid uptake and beta oxidation in adipose tissue while simultaneously decreasing hepatic lipid accumulation, increasing fatty acid oxidation and energy consumption [97]. Heart secreted peptides have been shown closely modulate liver metabolism and we aimed to identify potential peptides that were upregulated in our CA model that yielded an improved hepatic phenotype.

Secreted peptides have been characterized to regulate nearly all aspects of physiology and have been a focus for the diagnosis and treatment of adverse metabolic perturbations. About 3000 unique proteins are secreted in mice and in humans, accounting for about 16% of the protein coding genome [98]. Quantitative Endocrine Network Interaction Estimation (QENIE) was performed to identify heart secreted proteins, upregulated in CA mice, that had a regulatory role on CA liver gene expression by calculating correlative relationships between the two RNA sequence datasets. QENIE operates on the basis that, in a population, natural variation in transcript levels for most genes differ from one individual to another. Thus, inter-organ communication between two tissue types will also vary in a coordinated fashion whereby differences in an endocrine factor in a source tissue will show correlation with the responder genes in the target tissue [98]. By cross referencing found correlations to the Hybrid Mouse Diversity Panel HMDP database, previous clinical and physiological data could be utilized to predict clinical outcomes based on targets of the putative endocrine factors.

We narrowed down the identified cardiac secreted proteins to a select list of candidate proteins that will be validated experimentally. These proteins were all flagged as upregulated in the CA myocardium and were predicted to modulate the liver directly, based on predictive modeling of target genes. Some endocrine peptides were also predicted to have additional whole body metabolic effects, based on correlations with metabolic traits databases. Stand out regulators are described in depth below.

Annexin A1is ubiquitously expressed is found in secretory vesicles as well as other cellular compartments. Annexin A1 (Anxa1) regulates metabolic enzymes related to cell growth, differentiation, motility, and apoptosis. As a secretory protein, Anxa1 acts as an anti-inflammatory, pro-resolving protein which exerts its effects via binding to formyl peptide

receptor 2. AnxA1 KO mice were found to have enhanced liver inflammation and fibrosis, as well as increased weight gain accompanied by larger adipocytes. Moreover, Anxa1 KO mice displayed elevated glucose levels and reduced insulin sensitivity. When Anxa1 was overexpressed in the liver, M2 macrophage polarization was favored, resulting in protection from NASH [99].

Annexin A2 (Anaxa2) has prominent functions mediating insulin-stimulated translocation of GLUT4 in adipocytes and anti-inflammatory signaling. AnxA2 deficient animals had delayed clearance of fatty acids due to compromised CD36-mediated import from the bloodstream. Animal models of obesity suggested that Anaxa2 expression rise as a compensatory measure to higher energy intake [99]. While QENIE analysis predicted strong correlation to liver expression changes, more research is needed to determine its direct functions on hepatocytes.

Apolipoprotein E (ApoE) is a key component of triglyceride rich lipoproteins, such as VLDL and chylomicrons and is required for receptor mediated uptake of carrier contents. ApoE deficiency in mice has been shown to elevate plasma cholesterol concentration as well as dramatically increase hepatic fat accumulation due to dysfunctional transport of triglycerides and the inability to synthesize VLDL for export [100]. Its ubiquitous expression paired with direct effects on hepatic metabolism makes ApoE a good endocrine peptide candidate to test.

Paraoxonase-1 (Pon1) is an antioxidant enzyme with lactonase and esterase activity. Clinically, Pon1 concentration in the liver and serum are decreased in patients with liver diseases [101]. In vivo studies show overexpression to be protective against the development of liver inflammation and fibrosis. The proposed pathway is Pon1 inhibition of monocyte chemoattractant-1 (MCP-1). MCP-1 is a major driver of monocyte infiltration into tissues and is elevated in patients with chronic inflammatory diseases [101]. Increased expression of Pon1 by

the myocardium may therefore have anti-inflammatory roles in both the liver and in other organs.

Platelet factor 4 (Pf4) is a chemokine with anti-inflammatory roles. In patients and in mouse models of liver disease, serum concentration of Pf4 were lowered. Pf4 KO mice displayed increased liver damage due to high levels of hepatocyte apoptosis and an enhanced pro-inflammatory response by liver macrophages. Pf4 promotes the synthesis of activated protein C (APC), an inhibitor of monocytes and macrophages [102]. Resident and infiltrating hepatic macrophages are critical in the pathogenesis of liver injury and their suppression may attenuate liver disease.

Our model shows the close metabolic and regulatory relationships between the heart and liver. Mitochondrial Akt1 signaling is able to modulate some of these interconnected pathways. RNAseq allowed us to characterize the improve state of livers in CA mice, however expression data alone does not always correspond with protein expression and activity. To determine possible cardiokine regulation of the liver, higher level analysis was performed by calculating the correlation of endocrine source expression with their target gene expressions and referencing an established genetic variation and traits database. From the predicted endocrine peptides, we have discussed a selection of candidate peptides that will be tested in future investigations.

VI. Figures

Figure 4.1

CAMCAKT

A

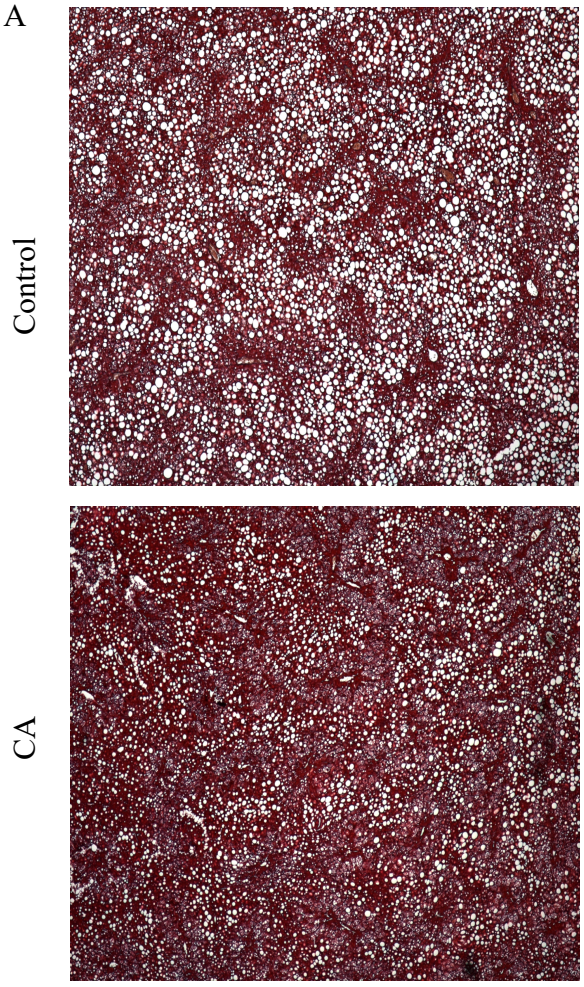

B.

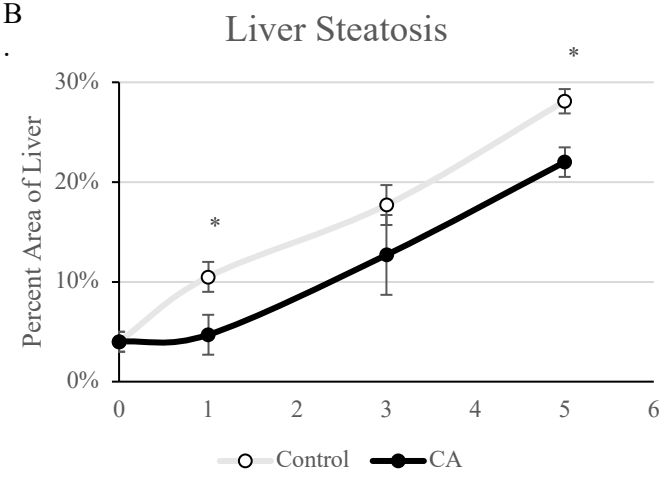

Figure 4.1 Cardiac mito-Akt1 Signaling Attenuates Liver Steatosis. Liver steatosis was quantified over multiple durations of HFF treatment. Representative images of HE stained liver sections after 5 months of HFF diet are shown (A). CA mice consistently exhibited reduced steatosis up to 5 months on HFF diet. (B) ($n = 12$, $*p < 0.05$).

Figure 4.2

CAMCAKT

A.

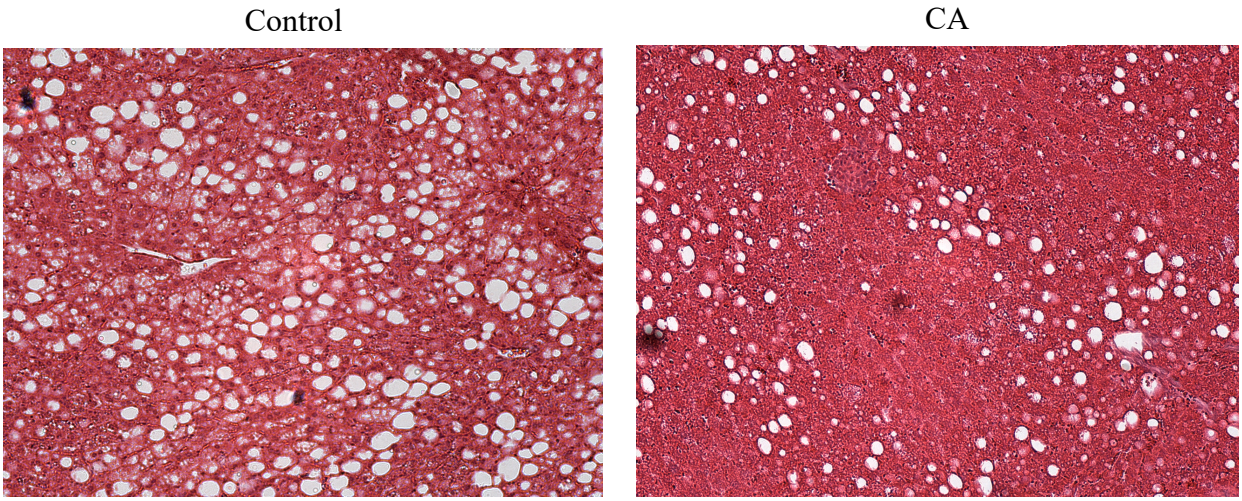

B.

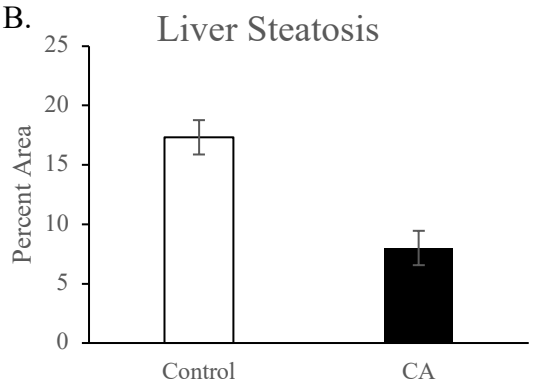

C.

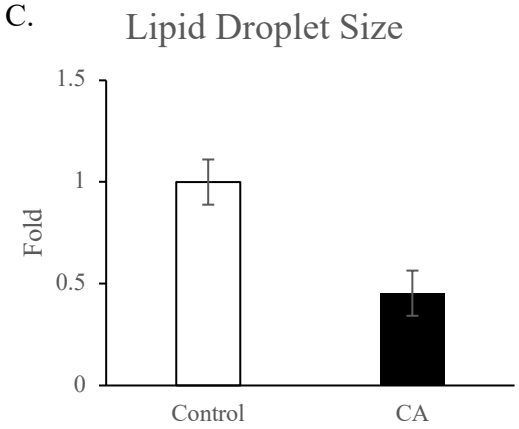

Figure 4.2 Cardiac mito-Akt1 Signaling Attenuates Liver Steatosis. Representative images of HE stained liver sections show reduced steatosis in CA mice after 2 months on HFF (A). Quantification of images revealed a 50% lower percent area of lipid droplets (B) and a 50% reduction in average droplet size (C) ($n = 12$, $*p < 0.05$).

Figure 4.3

CAMCAKT

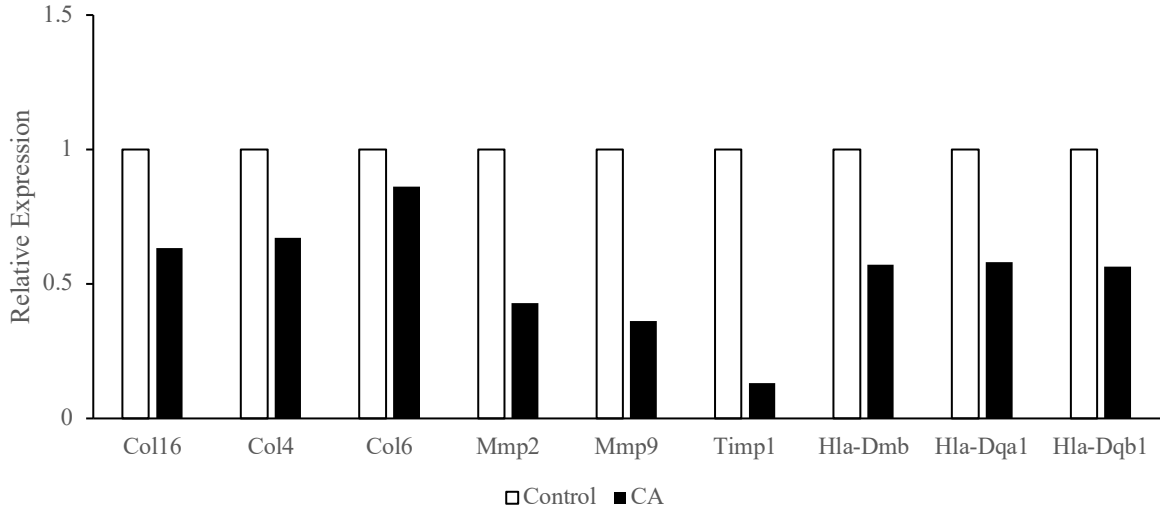

Figure 4.3 Cardiac mito-Akt1 Signaling Reduced Markers of NAFLD. RNA sequencing revealed that markers of NAFLD including isoforms of collagen, matrix metalloproteinases, and antigen presenting molecules are reduced in CA mice livers. (n = 6).

Figure 4.4

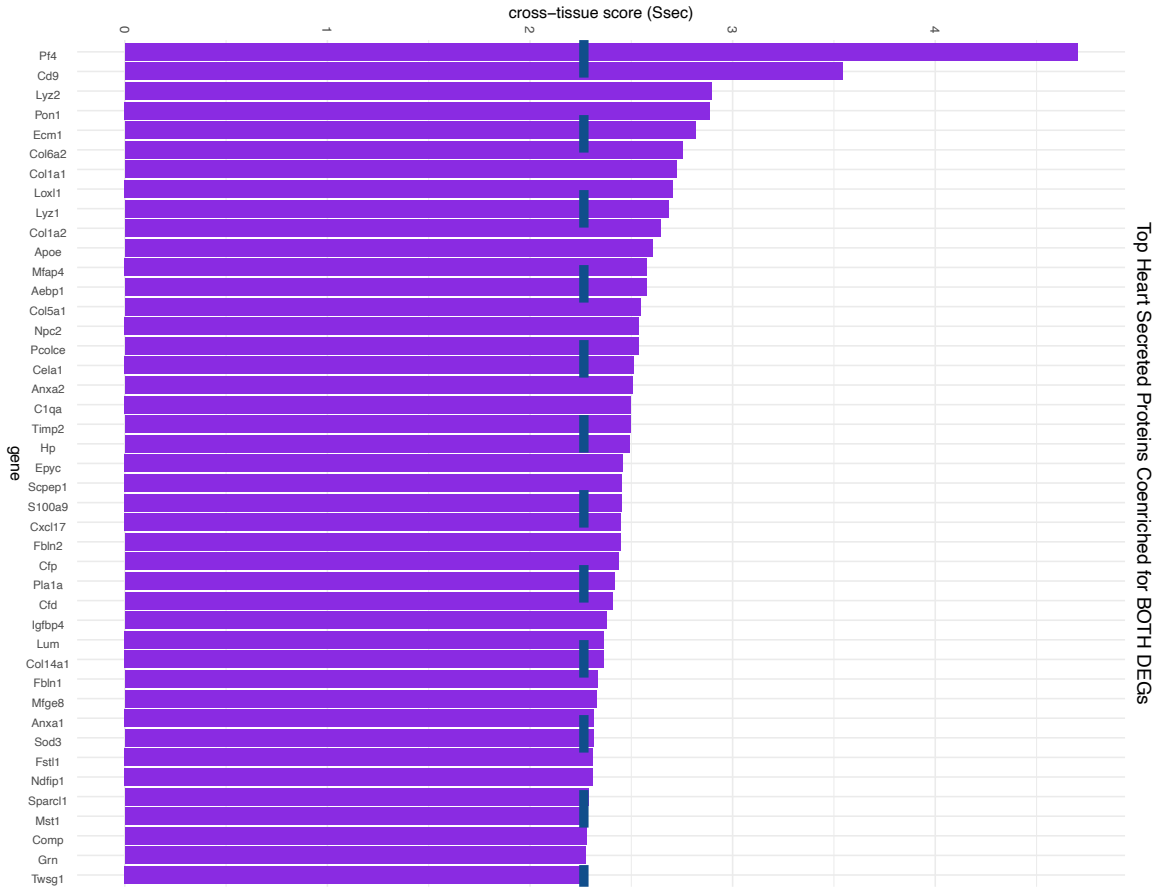

Figure 4.4 Cardiac mito-Akt1 Signaling Remotely Modulates Liver Metabolism Through Secreted Proteins. Cardiac secreted proteins, upregulated by mito-Akt1, targeting liver gene expression are predicted through QENIE analysis. Cross-tissue scores indicate strength of correlation.

Figure 4.5

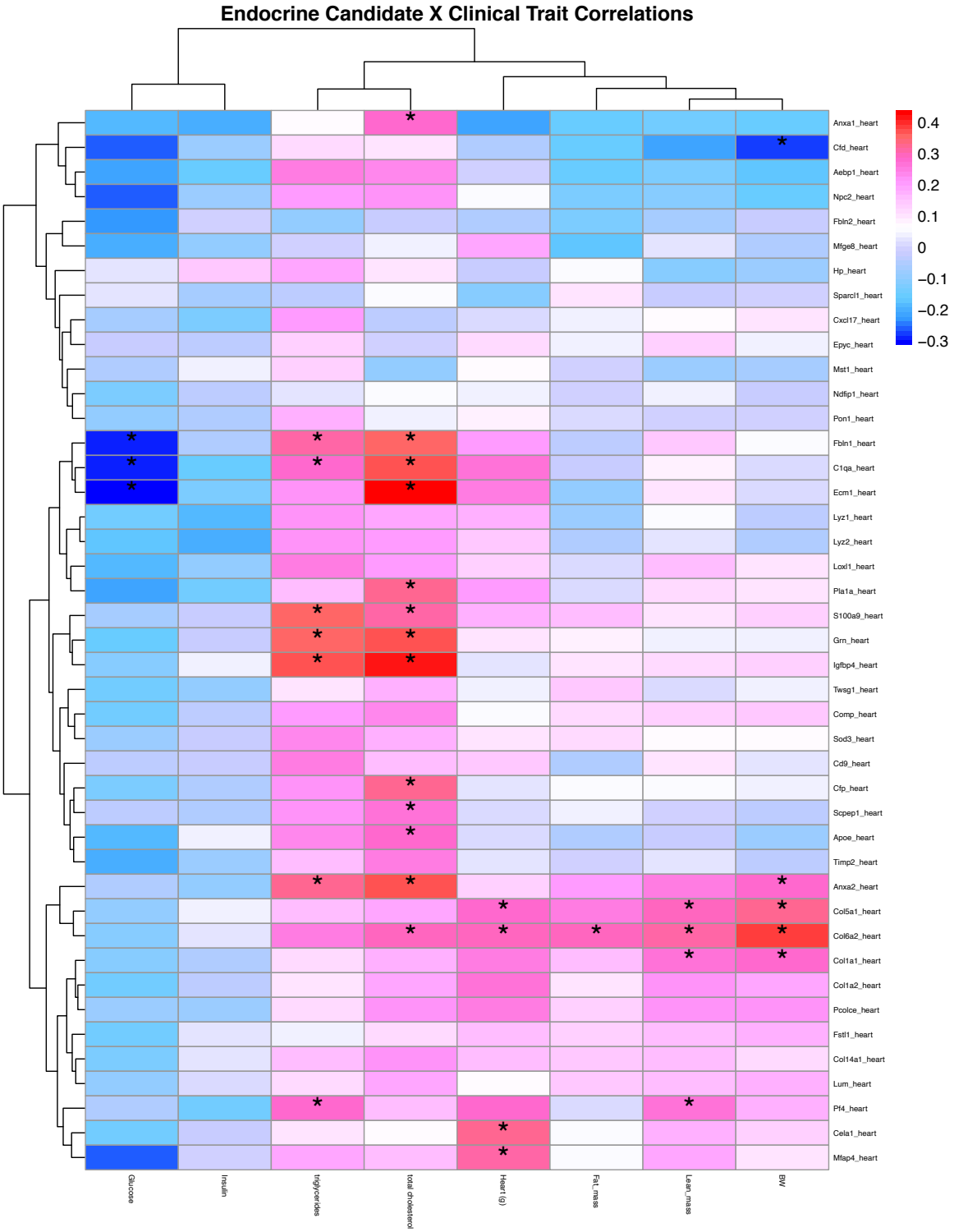
Endocrine Candidate X Clinical Trait Correlations
0.4
0.3
0.2
0.1
0
−0.1
−0.2
−0.3
Anxa1_heart
Cfd_heart
Aebp1_heart
Npc2_heart
Fbln2_heart
Mfge8_heart
Hp_heart
Sparcl1_heart
Cxcl17_heart
Epyc_heart
Mst1_heart
Ndfip1_heart
Pon1_heart
Fbln1_heart
C1qa_heart
Ecm1_heart
Lyz1_heart
Lyz2_heart
Loxl1_heart
Pla1a_heart
S100a9_heart
Grn_heart
Igfbp4_heart
Twsg1_heart
Comp_heart
Sod3_heart
Cd9_heart
Cfp_heart
Scpep1_heart
Apoe_heart
Timp2_heart
Anxa2_heart
Col5a1_heart
Col6a2_heart
Col1a1_heart
Col1a2_heart
Pcolce_heart
Fstl1_heart
Col14a1_heart
Lum_heart
Pf4_heart
Cela1_heart
Mfap4_heart
Glucose
Insulin
triglycerides
total cholesterol
Heart (g)
Fat_mass
Lean_mass
BW

Figure. 4.5 Cardiac mito-Akt1 Signaling Promotes Myocardial Secreted Proteins Regulating Whole Body Metabolism QENIE analysis of heart secreted proteins, upregulated by cardiac mito-Akt1, using HMDP clinical trait data, are correlated with changes in clinical traits. Positive correlation suggests clinical improvements of the listed traits.

CHAPTER 5

CONCLUSION

Cases of diabetic cardiomyopathy is increasing in prevalence, yet the underlying mechanisms are not clear. There remain no treatments to specifically target the physiopathology of diabetic cardiomyopathy thus more research is needed. Our lab has focused on mitochondrially targeted Akt1 signaling as a link between diabetes and cardiomyopathy. We demonstrated that insulin signaling deficiency or insensitivity impairs activation of Akt1 by PI3K, downstream of the insulin receptor. Loss of Akt1 signaling to mitochondria subsequently leads to mitochondrial dysfunction, characterized by dissociation of the ATP synthase complex, reduced ATP production, increased ROS production, and release of caspases. We demonstrated, in vivo, with a transgenic model of dominant negative mitochondrial Akt1 that impaired signaling leads to myocardial fibrosis, loss of heart function and heart failure.

We then demonstrated, using a transgenic model of constitutively active mitochondrial Akt1, that sustained Akt1 signaling can prevent development of cardiomyopathy in a diabetic setting. Under challenge from a high fat and high fructose diet induced model of obesity and diabetes, we showed that active mitochondrial Akt1 signaling was able to protect the myocardium from ventricular hypertrophy and improve heart function. Energetically, mitochondrial respiration efficiency was increased by a lowered oxygen consumption paired with greater ATP synthesis by reduced proton leak. Thus, constitutively active mitochondrial Akt1 protected the myocardium against diabetic cardiomyopathy

Analysis of gene expression suggested that mitochondrial Akt1 signaling increased metabolism of fatty acids. The result of which was measurable at the whole-body level by significant decrease in fat mass. Particularly during early development of diabetes, in additional to the improvement in body composition, whole body energy expenditure was measurably higher due to active mitochondrial Akt1 signaling. These data show that the heart, as a major consumer of energy, had a measurable impact on the whole-body level.

We finally focused on metabolic changes in the liver in the context of mitochondrial Akt1 signaling. The heart and liver are closely co-regulated and both are affected by metabolic syndrome and this was apparent in our model. While improvements in body composition diminished as body fat accumulated, liver steatosis was consistently attenuated. Markers of liver steatosis, fibrosis, and inflammation were decreased. To interrogate the regulatory link between the heart and liver, deeper analysis of gene correlation patterns was performed. We generated a selection of candidate heart secreted proteins that were predicted to modulate hepatic gene expression. These findings suggest that cardiac mitochondrial Akt1 signaling regulates liver metabolism with specificity via endocrine peptides in addition to increasing metabolic flux. Our future research aims to validate candidate peptides as cardiac regulators of hepatic metabolism (Figure 5.1).

Figure 5.1

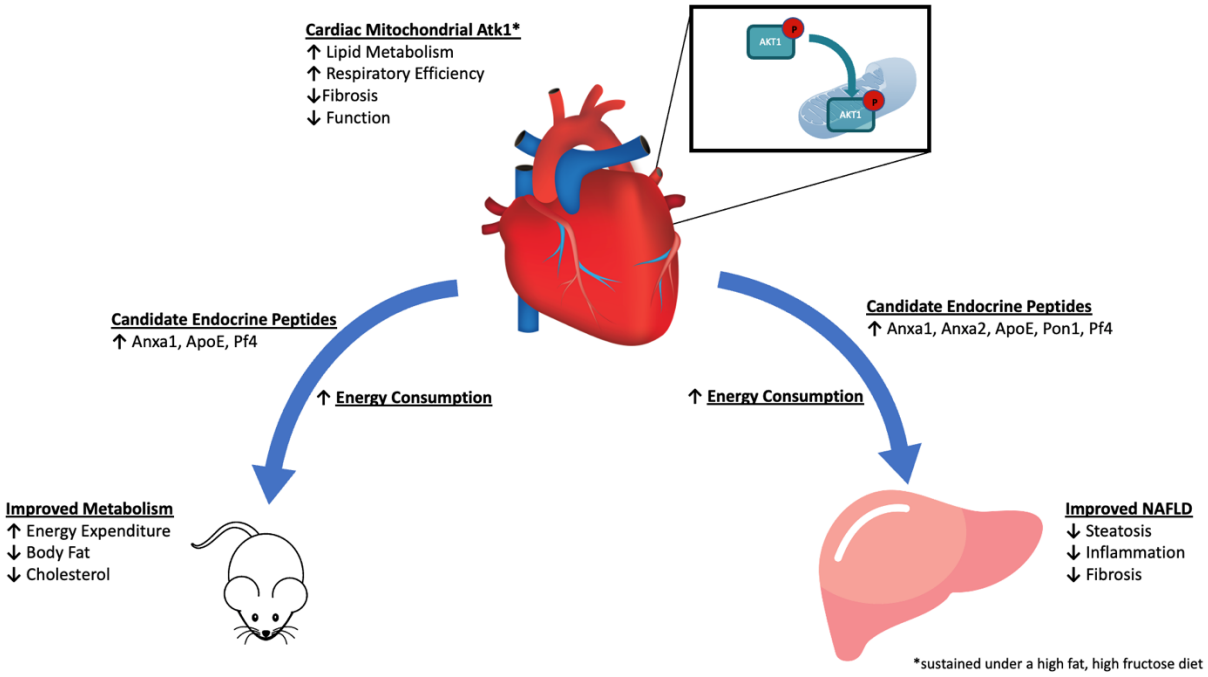

Figure 5.1 Overview of Cardiac Mitochondrial Akt1's Role in a Diet Induced Diabetic Setting

References

1. Kannel, W.B., M. Hjortland, and W.P. Castelli, *Role of diabetes in congestive heart failure: the Framingham study.* Am J Cardiol, 1974. **34**(1): p. 29-34.
2. Regan, T.J., et al., *Evidence for cardiomyopathy in familial diabetes mellitus.* J Clin Invest, 1977. **60**(4): p. 884-99.
3. *National Diabetes Statistics Report, 2020*. 2020.
4. Jia, G., et al., *Endothelial Mineralocorticoid Receptor Deletion Prevents Diet-Induced Cardiac Diastolic Dysfunction in Females.* Hypertension, 2015. **66**(6): p. 1159-1167.
5. Raev, D.C., *Which left ventricular function is impaired earlier in the evolution of diabetic cardiomyopathy? An echocardiographic study of young type I diabetic patients.* Diabetes Care, 1994. **17**(7): p. 633-9.
6. Lind, M., et al., *Glycaemic control and incidence of heart failure in 20,985 patients with type 1 diabetes: an observational study.* Lancet, 2011. **378**(9786): p. 140-6.
7. Bugger, H. and E.D. Abel, *Rodent models of diabetic cardiomyopathy.* Dis Model Mech, 2009. **2**(9-10): p. 454-66.
8. Jia, G., M.A. Hill, and J.R. Sowers, *Diabetic Cardiomyopathy: An Update of Mechanisms Contributing to This Clinical Entity.* Circ Res, 2018. **122**(4): p. 624-638.
9. Stratton, I.M., et al., *Association of glycaemia with macrovascular and microvascular complications of type 2 diabetes (UKPDS 35): prospective observational study.* Bmj, 2000. **321**(7258): p. 405-12.
10. Boyer, J.K., et al., *Prevalence of ventricular diastolic dysfunction in asymptomatic, normotensive patients with diabetes mellitus.* Am J Cardiol, 2004. **93**(7): p. 870-5.
11. Shivalkar, B., et al., *Flow mediated dilatation and cardiac function in type 1 diabetes mellitus.* Am J Cardiol, 2006. **97**(1): p. 77-82.
12. Fang, Z.Y., et al., *Screening for heart disease in diabetic subjects.* Am Heart J, 2005. **149**(2): p. 349-54.
13. Tschöpe, C., et al., *Transgenic activation of the kallikrein-kinin system inhibits intramyocardial inflammation, endothelial dysfunction and oxidative stress in experimental diabetic cardiomyopathy.* Faseb j, 2005. **19**(14): p. 2057-9.
14. Wu, K.K. and Y. Huan, *Diabetic atherosclerosis mouse models.* Atherosclerosis, 2007. **191**(2): p. 241-9.
15. Norton, G.R., G. Candy, and A.J. Woodiwiss, *Aminoguanidine prevents the decreased myocardial compliance produced by streptozotocin-induced diabetes mellitus in rats.* Circulation, 1996. **93**(10): p. 1905-12.
16. Aragno, M., et al., *Oxidative stress-dependent impairment of cardiac-specific transcription factors in experimental diabetes.* Endocrinology, 2006. **147**(12): p. 5967-74.
17. Shimizu, M., et al., *Collagen remodelling in myocardia of patients with diabetes.* J Clin Pathol, 1993. **46**(1): p. 32-6.
18. Chiu, J., et al., *PARP mediates structural alterations in diabetic cardiomyopathy.* J Mol Cell Cardiol, 2008. **45**(3): p. 385-93.
19. Van Linthout, S., et al., *Reduced MMP-2 activity contributes to cardiac fibrosis in experimental diabetic cardiomyopathy.* Basic Res Cardiol, 2008. **103**(4): p. 319-27.

20. Wang, J., et al., *Causes and characteristics of diabetic cardiomyopathy.* Rev Diabet Stud, 2006. **3**(3): p. 108-17.
21. Franssen, C., et al., *Myocardial Microvascular Inflammatory Endothelial Activation in Heart Failure With Preserved Ejection Fraction.* JACC Heart Fail, 2016. **4**(4): p. 312-24.
22. Vincent, M.A., et al., *Microvascular recruitment is an early insulin effect that regulates skeletal muscle glucose uptake in vivo.* Diabetes, 2004. **53**(6): p. 1418-23.
23. Anderson, E.J., et al., *Substrate-specific derangements in mitochondrial metabolism and redox balance in the atrium of the type 2 diabetic human heart.* J Am Coll Cardiol, 2009. **54**(20): p. 1891-8.
24. Randle, P.J., et al., *The glucose fatty-acid cycle. Its role in insulin sensitivity and the metabolic disturbances of diabetes mellitus.* Lancet, 1963. **1**(7285): p. 785-9.
25. Kim, J.A., Y. Wei, and J.R. Sowers, *Role of mitochondrial dysfunction in insulin resistance.* Circ Res, 2008. **102**(4): p. 401-14.
26. Teshima, Y., et al., *Production of reactive oxygen species in the diabetic heart. Roles of mitochondria and NADPH oxidase.* Circ J, 2014. **78**(2): p. 300-6.
27. Giacco, F. and M. Brownlee, *Oxidative stress and diabetic complications.* Circ Res, 2010. **107**(9): p. 1058-70.
28. Van den Bergh, A., et al., *Dyslipidaemia in type II diabetic mice does not aggravate contractile impairment but increases ventricular stiffness.* Cardiovasc Res, 2008. **77**(2): p. 371-9.
29. Belke, D.D., E.A. Swanson, and W.H. Dillmann, *Decreased sarcoplasmic reticulum activity and contractility in diabetic db/db mouse heart.* Diabetes, 2004. **53**(12): p. 3201-8.
30. Ye, G., et al., *Metallothionein prevents diabetes-induced deficits in cardiomyocytes by inhibiting reactive oxygen species production.* Diabetes, 2003. **52**(3): p. 777-83.
31. Wallace, D.C., *Mitochondrial genetics: a paradigm for aging and degenerative diseases?* Science, 1992. **256**(5057): p. 628-32.
32. Jia, G., V.G. DeMarco, and J.R. Sowers, *Insulin resistance and hyperinsulinaemia in diabetic cardiomyopathy.* Nat Rev Endocrinol, 2016. **12**(3): p. 144-53.
33. Loncarevic, B., et al., *Silent diabetic cardiomyopathy in everyday practice: a clinical and echocardiographic study.* BMC Cardiovasc Disord, 2016. **16**(1): p. 242.
34. van der Leeuw, J., et al., *Novel Biomarkers to Improve the Prediction of Cardiovascular Event Risk in Type 2 Diabetes Mellitus.* J Am Heart Assoc, 2016. **5**(6).
35. Wolf, P., et al., *Suppression of plasma free fatty acids reduces myocardial lipid content and systolic function in type 2 diabetes.* Nutr Metab Cardiovasc Dis, 2016. **26**(5): p. 387-92.
36. Eurich, D.T., et al., *Benefits and harms of antidiabetic agents in patients with diabetes and heart failure: systematic review.* Bmj, 2007. **335**(7618): p. 497.
37. Yang, J.Y., et al., *Insulin stimulates Akt translocation to mitochondria: implications on dysregulation of mitochondrial oxidative phosphorylation in diabetic myocardium.* J Mol Cell Cardiol, 2009. **46**(6): p. 919-26.
38. Yang, J.Y., et al., *Impaired translocation and activation of mitochondrial Akt1 mitigated mitochondrial oxidative phosphorylation Complex V activity in diabetic myocardium.* J Mol Cell Cardiol, 2013. **59**: p. 167-75.

39. Nasir, S. and D. Aguilar, *Congestive heart failure and diabetes mellitus: balancing glycemic control with heart failure improvement.* Am J Cardiol, 2012. **110**(9 Suppl): p. 50b-57b.
40. Gaggin, H.K. and J.L. Januzzi, Jr., *Biomarkers and diagnostics in heart failure.* Biochim Biophys Acta, 2013. **1832**(12): p. 2442-50.
41. Brandt, R.R., et al., *Atrial natriuretic peptide in heart failure.* J Am Coll Cardiol, 1993. **22**(4 Suppl A): p. 86a-92a.
42. Peter, A.K., et al., *Expression of Normally Repressed Myosin Heavy Chain 7b in the Mammalian Heart Induces Dilated Cardiomyopathy.* J Am Heart Assoc, 2019. **8**(15): p. e013318.
43. Boudina, S., et al., *Reduced mitochondrial oxidative capacity and increased mitochondrial uncoupling impair myocardial energetics in obesity.* Circulation, 2005. **112**(17): p. 2686-95.
44. Crescenzo, R., et al., *Mitochondrial efficiency and insulin resistance.* Front Physiol, 2014. **5**: p. 512.
45. Goldenberg, J.R., et al., *Preservation of Acyl Coenzyme A Attenuates Pathological and Metabolic Cardiac Remodeling Through Selective Lipid Trafficking.* Circulation, 2019. **139**(24): p. 2765-2777.
46. Son, N.H., et al., *PPARγ-induced cardiolipotoxicity in mice is ameliorated by PPARα deficiency despite increases in fatty acid oxidation.* J Clin Invest, 2010. **120**(10): p. 3443-54.
47. Ellis, J.M., et al., *Mouse Cardiac Acyl Coenzyme A Synthetase 1 Deficiency Impairs Fatty Acid Oxidation and Induces Cardiac Hypertrophy.* Molecular and Cellular Biology, 2011. **31**(6): p. 1252-1262.
48. Schulze, P.C., K. Drosatos, and I.J. Goldberg, *Lipid Use and Misuse by the Heart.* Circulation Research, 2016. **118**(11): p. 1736-1751.
49. Guo, Z., et al., *Cardiac expression of adiponectin and its receptors in streptozotocin-induced diabetic rats.* Metabolism, 2007. **56**(10): p. 1363-71.
50. Razani, B., et al., *Fatty acid synthase modulates homeostatic responses to myocardial stress.* J Biol Chem, 2011. **286**(35): p. 30949-30961.
51. Jones, D.S., S.H. Podolsky, and J.A. Greene, *The burden of disease and the changing task of medicine.* N Engl J Med, 2012. **366**(25): p. 2333-8.
52. An, R., *Prevalence and Trends of Adult Obesity in the US, 1999-2012.* ISRN Obes, 2014. **2014**: p. 185132.
53. Skinner, A.C. and J.A. Skelton, *Prevalence and trends in obesity and severe obesity among children in the United States, 1999-2012.* JAMA Pediatr, 2014. **168**(6): p. 561-6.
54. McAllister, E.J., et al., *Ten putative contributors to the obesity epidemic.* Crit Rev Food Sci Nutr, 2009. **49**(10): p. 868-913.
55. Shen, W., et al., *Adipose tissue quantification by imaging methods: a proposed classification.* Obes Res, 2003. **11**(1): p. 5-16.
56. Grant, R.W. and V.D. Dixit, *Adipose tissue as an immunological organ.* Obesity (Silver Spring), 2015. **23**(3): p. 512-8.
57. Wadden, T.A. and D.B. Sarwer, *Behavioral assessment of candidates for bariatric surgery: a patient-oriented approach.* Obesity (Silver Spring), 2006. **14 Suppl 2**: p. 53s-62s.

58. *Expert Panel Report: Guidelines (2013) for the management of overweight and obesity in adults.* Obesity (Silver Spring), 2014. **22 Suppl 2**: p. S41-410.
59. Heymsfield, S.B. and T.A. Wadden, *Mechanisms, Pathophysiology, and Management of Obesity.* N Engl J Med, 2017. **376**(3): p. 254-266.
60. Gylling, H., et al., *Insulin sensitivity regulates cholesterol metabolism to a greater extent than obesity: lessons from the METSIM Study.* J Lipid Res, 2010. **51**(8): p. 2422-7.
61. Younossi, Z.M., et al., *Global epidemiology of nonalcoholic fatty liver disease-Meta-analytic assessment of prevalence, incidence, and outcomes.* Hepatology, 2016. **64**(1): p. 73-84.
62. Ghevariya, V., et al., *Knowing What's Out There: Awareness of Non-Alcoholic Fatty Liver Disease.* Front Med (Lausanne), 2014. **1**: p. 4.
63. Bambha, K., et al., *Ethnicity and nonalcoholic fatty liver disease.* Hepatology, 2012. **55**(3): p. 769-80.
64. Wong, R.J., et al., *Nonalcoholic steatohepatitis is the second leading etiology of liver disease among adults awaiting liver transplantation in the United States.* Gastroenterology, 2015. **148**(3): p. 547-55.
65. Donnelly, K.L., et al., *Sources of fatty acids stored in liver and secreted via lipoproteins in patients with nonalcoholic fatty liver disease.* J Clin Invest, 2005. **115**(5): p. 1343-51.
66. Schwarz, J.M., et al., *Hepatic de novo lipogenesis in normoinsulinemic and hyperinsulinemic subjects consuming high-fat, low-carbohydrate and low-fat, high-carbohydrate isoenergetic diets.* Am J Clin Nutr, 2003. **77**(1): p. 43-50.
67. Sunny, N.E., et al., *Excessive hepatic mitochondrial TCA cycle and gluconeogenesis in humans with nonalcoholic fatty liver disease.* Cell Metab, 2011. **14**(6): p. 804-10.
68. Wong, V.W., et al., *Disease progression of non-alcoholic fatty liver disease: a prospective study with paired liver biopsies at 3 years.* Gut, 2010. **59**(7): p. 969-74.
69. Tilg, H. and A.R. Moschen, *Evolution of inflammation in nonalcoholic fatty liver disease: the multiple parallel hits hypothesis.* Hepatology, 2010. **52**(5): p. 1836-46.
70. Feldstein, A.E., et al., *Hepatocyte apoptosis and fas expression are prominent features of human nonalcoholic steatohepatitis.* Gastroenterology, 2003. **125**(2): p. 437-43.
71. Idrissova, L., et al., *TRAIL receptor deletion in mice suppresses the inflammation of nutrient excess.* J Hepatol, 2015. **62**(5): p. 1156-63.
72. Marra, F. and F. Tacke, *Roles for chemokines in liver disease.* Gastroenterology, 2014. **147**(3): p. 577-594.e1.
73. Leroux, A., et al., *Toxic lipids stored by Kupffer cells correlates with their pro-inflammatory phenotype at an early stage of steatohepatitis.* J Hepatol, 2012. **57**(1): p. 141-9.
74. Tacke, F. and H. Yoneyama, *From NAFLD to NASH to fibrosis to HCC: role of dendritic cell populations in the liver.* Hepatology, 2013. **58**(2): p. 494-6.
75. Ganz, M. and G. Szabo, *Immune and inflammatory pathways in NASH.* Hepatol Int, 2013. **7 Suppl 2**(Suppl 2): p. 771-81.
76. Ekstedt, M., et al., *Long-term follow-up of patients with NAFLD and elevated liver enzymes.* Hepatology, 2006. **44**(4): p. 865-73.
77. Agopian, V.G., et al., *Liver transplantation for nonalcoholic steatohepatitis: the new epidemic.* Ann Surg, 2012. **256**(4): p. 624-33.

78. National Guideline, C., *National Institute for Health and Care Excellence: Guidance*, in *Non-Alcoholic Fatty Liver Disease: Assessment and Management*. 2016, National Institute for Health and Care Excellence (UK)
Copyright © National Institute for Health and Care Excellence 2016.: London.
79. Fedchuk, L., et al., *Performance and limitations of steatosis biomarkers in patients with nonalcoholic fatty liver disease.* Aliment Pharmacol Ther, 2014. **40**(10): p. 1209-22.
80. Karlas, T., et al., *Individual patient data meta-analysis of controlled attenuation parameter (CAP) technology for assessing steatosis.* J Hepatol, 2017. **66**(5): p. 1022-1030.
81. Alkhouri, N. and A.E. Feldstein, *Noninvasive diagnosis of nonalcoholic fatty liver disease: Are we there yet?* Metabolism, 2016. **65**(8): p. 1087-95.
82. Tiikkainen, M., et al., *Effects of rosiglitazone and metformin on liver fat content, hepatic insulin resistance, insulin clearance, and gene expression in adipose tissue in patients with type 2 diabetes.* Diabetes, 2004. **53**(8): p. 2169-76.
83. Yki-Järvinen, H., *Thiazolidinediones.* N Engl J Med, 2004. **351**(11): p. 1106-18.
84. Ben-Shlomo, S., et al., *Glucagon-like peptide-1 reduces hepatic lipogenesis via activation of AMP-activated protein kinase.* J Hepatol, 2011. **54**(6): p. 1214-23.
85. Vilar-Gomez, E., et al., *Weight Loss Through Lifestyle Modification Significantly Reduces Features of Nonalcoholic Steatohepatitis.* Gastroenterology, 2015. **149**(2): p. 367-78.e5; quiz e14-5.
86. Hemmann, S., et al., *Expression of MMPs and TIMPs in liver fibrosis - a systematic review with special emphasis on anti-fibrotic strategies.* J Hepatol, 2007. **46**(5): p. 955-75.
87. Naim, A., Q. Pan, and M.S. Baig, *Matrix Metalloproteinases (MMPs) in Liver Diseases.* J Clin Exp Hepatol, 2017. **7**(4): p. 367-372.
88. Knittel, T., et al., *Expression patterns of matrix metalloproteinases and their inhibitors in parenchymal and non-parenchymal cells of rat liver: regulation by TNF-alpha and TGF-beta1.* J Hepatol, 1999. **30**(1): p. 48-60.
89. Han, Y.P., et al., *Essential role of matrix metalloproteinases in interleukin-1-induced myofibroblastic activation of hepatic stellate cell in collagen.* J Biol Chem, 2004. **279**(6): p. 4820-8.
90. Parola, M. and G. Robino, *Oxidative stress-related molecules and liver fibrosis.* J Hepatol, 2001. **35**(2): p. 297-306.
91. Giannelli, G., et al., *Antifibrogenic effect of IFN-alpha2b on hepatic stellate cell activation by human hepatocytes.* J Interferon Cytokine Res, 2006. **26**(5): p. 301-8.
92. Roderfeld, M., et al., *Cytokine blockade inhibits hepatic tissue inhibitor of metalloproteinase-1 expression and up-regulates matrix metalloproteinase-9 in toxic liver injury.* Liver Int, 2006. **26**(5): p. 579-86.
93. Iredale, J.P., *Tissue inhibitors of metalloproteinases in liver fibrosis.* Int J Biochem Cell Biol, 1997. **29**(1): p. 43-54.
94. Iredale, J.P., et al., *Tissue inhibitor of metalloproteinase-1 messenger RNA expression is enhanced relative to interstitial collagenase messenger RNA in experimental liver injury and fibrosis.* Hepatology, 1996. **24**(1): p. 176-84.
95. Russell, M.A., et al., *HLA Class II Antigen Processing and Presentation Pathway Components Demonstrated by Transcriptome and Protein Analyses of Islet β-Cells From Donors With Type 1 Diabetes.* Diabetes, 2019. **68**(5): p. 988-1001.

96. Kobayashi, H., et al., *Hepatic overexpression of MHC class II antigens and macrophage-associated antigens (CD68) in patients with biliary atresia of poor prognosis.* J Pediatr Surg, 1997. **32**(4): p. 590-3.
97. Nakamura, M. and J. Sadoshima, *Heart over mind: metabolic control of white adipose tissue and liver.* EMBO Mol Med, 2014. **6**(12): p. 1521-4.
98. Seldin, M.M., et al., *A Strategy for Discovery of Endocrine Interactions with Application to Whole-Body Metabolism.* Cell Metab, 2018. **27**(5): p. 1138-1155.e6.
99. Grewal, T., et al., *Annexins in Adipose Tissue: Novel Players in Obesity.* Int J Mol Sci, 2019. **20**(14).
100. Mensenkamp, A.R., et al., *Apolipoprotein E participates in the regulation of very low density lipoprotein-triglyceride secretion by the liver.* J Biol Chem, 1999. **274**(50): p. 35711-8.
101. Marsillach, J., et al., *Paraoxonase-1 is related to inflammation, fibrosis and PPAR delta in experimental liver disease.* BMC Gastroenterol, 2009. **9**: p. 3.
102. Drescher, H.K., et al., *Platelet Factor 4 Attenuates Experimental Acute Liver Injury in Mice.* Front Physiol, 2019. **10**: p. 326.